University of Pretoria

Tyre Force Prediction from Deformation Measurements

by

Robin Grant Gast

Submitted in partial fulfilment of the requirements for the degree

Master of Engineering
(Mechanical & Aeronautical Engineering)

in the Faculty of

Engineering, Built Environment and Information Technology (EBIT)

at the

University of Pretoria,
Pretoria

April 2022

Abstract

Tyre forces are the primary external forces applied to a vehicle, especially at lower speeds, but are notoriously difficult to measure or predict. An intelligent tyre which allows the external forces to be determined from simple measurements can be used to improve vehicle safety systems like ABS and stability control, and therefore reduce and even prevent road fatalities. If such a system can also predict the tyre-terrain pressure distribution then this will enable better modelling of the interaction between a tyre and deformable terrain, which is a particularly challenging aspect of terramechanics.

Tyres have highly non-linear behaviour due to complex geometry and construction, nearly incompressible materials, and the frictional interaction between the tyre and the road. Tyre modelling is a mature field but models that cater to the intelligent tyre are in their infancy, with much of the research only applicable to a narrow domain. Uncertainties in the relationship between the measurements that can be taken of the tyre and the tyre-road interaction make it clear that physical models have the highest likelihood of successfully investigating the identifiability of these forces. The relationship between strain and displacement measurements on the inner surface of the tyre and the external loads that caused them is not well understood, and this thesis explores the relationship between these quantities. The feasibility of determining external forces from strain or deformation measurements is investigated using a virtual experiment to isolate the problem from measurement capabilities.

Two finite element models of a tyre are developed to generate data to aid the study - one with reduced geometry and simplified boundary conditions, and another which models a full tyre. The reduced geometry model is modelled without internal air pressure, therefore it intentionally presents exaggerated deformations which is theorized to expose the sensitivity of the problem. The second model is more representative of the real tyre on which it is based, and is shown to correlate well with experimental vertical stiffness test results. Virtual Experiments are generated with the two models where the conditions can be tightly controlled. These virtual experiments are used in the inverse analysis as a substitute for measurements from real experiments, which means that the true answers are always known for all parameters.

A naïve optimisation-based virtual inverse simulation is solved to identify external forces which cause internal strains and deformations which match those of a corresponding virtual experiment. This study used the reduced geometry model in each optimisation loop to solve the virtual inverse problem. An identifiability study conducted using this method revealed that there are many local minima in the design space, especially when there is measurement noise present or if the initial guess of the external forces is not close to the true answer. These local minima make it difficult to dis-

tinguish between many statically equivalent solutions, and therefore the method is likely to converge to a solution which has an accurate total force but a poor estimation of the individual forces in the contact patch. An appropriate regularization strategy was implemented to prevent this.

Each virtual inverse simulation requires many hundreds of individual FEM simulations to converge to an answer, but only the data from the final solution is used. Therefore a data-driven approach is presented which uses a small dataset of full geometry virtual experiments to investigate how informative the data itself is. The dataset comprised of simulations where only the total deformation of the tyre was varied. A Principal Component Analysis is performed which clearly indicates that the problem is nearly one dimensional, since the first principal component explains the vast majority of the variance in the solution. This principal component analysis also reveals that deformation and strains measurements are informative in different ways, which can be used to inform regularization strategies for future work. A model was developed using Principal Component Regression to predict the external nodal forces from the internal deformations or strains. This model showed that although there is a single latent variable in the data, the non-linearity inherent in the problem requires at least three principal components to be used to successfully model the problem.

Principal component regression assumes that the direction of maximum variance in the input corresponds with the output, which may not always be true. Partial-Least Squares Regression is a similar method to principal component regression but overcomes this problem. Partial-least squares regression was used to map the internal deformations and strains to the output and was found to explain the variance in the data better with fewer components. This method was used to repeat the optimisation-based sensitivity study in a way that is not affected by the initial guess. Similar results to the previous study were found wherein the total forces are easy to predict but the distribution thereof is less identifiable. This method was used to map the identifiability of the external forces over the whole contact patch by sampling from a noisy measurement, predicting the forces, and repeating this process many times. Finally, this analysis was extended to show the relationship between the level of uncertainty in the measurements versus the effect on the identifiability of the external forces.

Acknowledgements

A number of people have given me considerable support and guidance, and deserve mention:

- My father who provided me with a passion for vehicles and more than everything I needed to ensure that I may complete my studies
- My late mother who set me on this path many years ago but was never afforded the opportunity to see the results of her efforts
- Professor Els, Professor Kok, Professor Wilke, and Dr Botha for the many hours of excellent guidance, without which this work would not have been remotely possible. It is a privilege and a pleasure to work with such knowledgeable and kind people
- My partner Alyssa whose endless support is truly a gift
- The Vehicle Dynamics Group for providing both the opportunity to study further and what feels like a second family

This document was typeset in LaTeX 2_ε

Contents

List of Figures

List of Tables

List of Symbols

Roman Symbols

Symbol	Description	Units
F_x	Longitudinal Tyre Force	N
F_y	Lateral Tyre Force	N
F_z	Vertical Tyre Force	N
$\boldsymbol{K}$	Covariance	-
k	Grouping of data	-
M	Number of strain nodes	-
M_x	Moment about x-axis	Nm
M_y	Moment about y-axis	Nm
N	Number of displacement nodes	-
r^*	Number of columns chosen for PCR	-
$\boldsymbol{T}$	Cross-covariance	-
$\boldsymbol{U}$	Nodal Displacement	mm
U_x	Longitudinal Nodal Deformation	mm
U_y	Lateral Nodal Deformation	mm
U_z	Vertical Nodal Deformation	mm
$\boldsymbol{V}$	SVD Component ("eigen-forces")	-
$\boldsymbol{W}$	SVD Component ("eigen-deformations/strains")	-
$\boldsymbol{x}$	Design Vector (External Forces)	N
$\boldsymbol{X}_\epsilon$	Input matrix of nodal strains	-
$\boldsymbol{X}_U$	Input matrix of nodal displacements	-
$\boldsymbol{Y}$	Output matrix of nodal reaction forces	-
$\boldsymbol{Z}$	Principal Component Score	-

Greek Symbols

Symbol	Description	Units
$\boldsymbol{\alpha}$	PCR weights	-
$\boldsymbol{\Sigma}$	SVD Component	-
$\boldsymbol{\epsilon}$	Strain Tensor	-
ϵ_{xx}	xx Strain Tensor Component	-
ϵ_{yy}	yy Strain Tensor Component	-
ϵ_{xy}	xy Strain Tensor Component	-
ν	Poisson's Ratio	-

List of Abbreviations

Abbreviation	Description
ADAS	Advanced Driver Assistance Systems
CAD	Computer-Aided Design
CST	Constant-Strain Triangle
DIC	Digital Image Correlation
FEM	Finite Element Method / Finite Element Model
FRTM	Flexible Ring Tyre Model
LI	Load Index
MEM	Modal Expansion Method
PCA	Principal Component Analysis
PCR	Principal Component Regression
PLS	Partial-Least Squares
PLSR	Partial-Least Squares Regression
RMOD-K	Comfort and Durability Tire (model)
RMSE	Root-Mean-Square Error
STTR	Static Tyre Test Rig
SVD	Singular Value Decomposition
T2Cam	Tyre-Terrain Camera
TYDEX	TYre Data EXchange Format
WFT	Wheel Force Transducer

Chapter 1

Introduction

1.1 Motivation and Problem Statement

The pneumatic tyre has been the subject of much study since its invention which can be attributed to that fact that it is the primary mechanism by which external forces act on a vehicle, especially at lower speeds where aerodynamic effects are not significant. The complex construction of the modern tyre, as well as its frictional interaction with the road surface, contribute to the difficulty in modelling and predicting the force generation of the tyre. Road accidents are 2-3 times more likely to occur in rainy conditions (Brodsky and Hakkert, 1988), indicating that humans are poor at estimating the maximum force that a tyre can produce. Road conditions are generally unpredictable and have a significant influence on the behaviour of tyres, further complicating the development of Advanced Driver Assistance Systems (ADAS). For example optimal braking is often modelled and controlled based on the longitudinal slip of the tyre since this quantity can be estimated readily (Tsiotras and De Wit, 2000), but it is clear that if one can instead accurately estimate the tyre force directly then ADAS will perform significantly better. Additionally, the capability to accurately predict the tyre-terrain pressure distribution is invaluable in terramechanics studies. We therefore seek a system or strategy that can estimate tyre force accurately and over a wide range of driving conditions in order to further the development of ADAS and ultimately save lives.

Previous research efforts at the University of Pretoria have led to the development of the Tyre-Terrain Camera System (T2Cam) (Guthrie et al., 2017; Feldesi et al., 2020; Pegram et al., 2021), which can measure full-field deformation and strain of the inner surface of a tyre in the region of the contact patch using stereovision. T2Cam therefore has the potential to be used

as an intelligent tyre sensor, but the appropriate modelling strategy to accomplish tyre force prediction has yet to be determined. Much of the existing research in modelling is empirical but ideally a physics-based model should be used for research and development. Moreover, it remains unknown whether or not there exists a unique solution to such a problem in general. Saint Venant's principle dictates that the effects of statically equivalent loads becomes similar at sufficiently large distances from the load application, and as such it is expected that it may be challenging to identify the distribution of external tyre forces by measuring the deformations and strains at a different location. The problem statement is thus *"Is it possible to identify a unique distribution of external forces acting on a tyre by measuring strain or deformation on the inner surface of the tyre?"*.

1.2 Motivation and Goals

While some models and procedures do exist to predict tyres forces from measurements on a tyre in specific scenarios, there has been little research into whether these solutions are guaranteed to exist. This thesis aims to determine whether or not it is possible to determine the external forces acting on a particular tyre if only the deformations and strains on the inner surface of the tyre are known, and if so to what degree these forces are identifiable. This work also aims to determine to what degree sensor noise influences the identifiability of these external forces.

1.3 Thesis Outline

In Chapter 2 the concept of an intelligent or smart tyre is introduced, as well as a prototype intelligent tyre developed at the University of Pretoria. A review of tyre models developed for intelligent tyre research follows and a tyre is chosen for the study. Finally, the chosen axis system is introduced.

In Chapter 3 two coarse finite element models are developed to be used for the studies that follow. The first model has reduced geometry and boundary conditions, while the second model is representative of a real tyre. The models are developed in the open-source finite element analysis application CalculiX (Guido Dhondt, Klaus Wittig, 1998) with a mesh generated by the open-source mesh generator gmsh (Geuzaine and Remacle, 2009).

A naïve optimisation-based virtual inverse problem is developed in Chapter 4 to investigate the identifiability of external forces using the reduced geometry model. Three studies were conducted to assess how well such a virtual inverse problem identifies external forces with and without measurement noise, as well as in the scenario where the initial guess is poor. The inverse problem is solved in MATLAB (The Mathworks, Inc., 2020) as a "FEM-in-the-loop" with one of the models developed in Chapter 3.

A data-driven approach to make more intelligent use of the information from the virtual experiments is implemented in Chapter 5 using Principal Component Analysis. The interpretation of this analysis allows one to formulate regularization strategies to alleviate the problems encountered in the previous chapter. Additionally, the methods developed in Chapter 5 can be used to develop better intelligent tyre hardware.

The research is summarized in Chapter 6. A number of suggestions are recommended for future work in this field.

Chapter 2

Literature Study

2.1 The Tyre as a Sensor

The idea of using the tyre as a sensor is not a new one, however commercial implementations of intelligent tyre concepts are currently limited to wear-focused solutions. For example Continental Tires* offers a wide range of their tyres with an integrated pressure and temperature monitoring sensor system, which can be either supplied with the tyre or fitted at a later stage. While the term "intelligent tyre" has not yet been rigidly described it can be said that an intelligent tyre is a system where a standard tyre and/or rim is fitted some sensor system to provide measurements. Some intelligent tyre concepts go further as to predict tyre kinematic or dynamic properties, such as slip angle or lateral force.

There has been significant research devoted to investigating the suitability of various sensors for further developing the sensing capability of a tyre. It is clear that the real challenge in developing an intelligent tyre lies as much in using sensor data as it does in the design of the concept, which is evident by the fact that the subset of intelligent tyre concepts which have been used to predict tyre force is small. The European Commission (2005, 2008) launched two projects in the early 2000's, called APOLLO and FRICTI@N respectively to investigate the possibility of an intelligent tyre. The APOLLO project investigated largely the various configurations of existing technologies, while FRICTI@N further developed the concept by including the necessary tyre modelling aspects for real-time friction estimation. APOLLO identified 3 classes of appropriate

*https://www.continental-tires.com/transport/products/continental-itire

sensing solutions being acceleration sensors, optical sensors, and strain sensors. Based on the potential of each class to identify tyre lateral, longitudinal, and vertical force it was determined that optical sensors have the highest potential, with the largest drawback being their large power consumption. The major attraction of optical sensors is the possibility of measuring full-field displacement and strain rather than just point measurements which are common of the strain-based and acceleration-based approaches. The optical approach was therefore taken in the development of T2Cam as its research potential is clearly the highest, where a stereo-vision camera system was chosen as the measurement device. APOLLO and FRICTI@N demonstrated that an intelligent tyre concept was feasible with existing technology, but highlighted that the missing link is an appropriate way to interpret the data obtained by an intelligent tyre.

2.2 Tyre-Terrain Camera (T2Cam)

Using Digital Image Correlation (DIC) techniques, Guthrie et al. (2017) developed an intelligent tyre concept called the Tyre-Terrain Camera (T2Cam) where a set of stabilised stereovision cameras were mounted in a specially designed split-ring rim. The system is used to generate a 3D point-cloud of the deformation of the inner surface of the tyre in the region of the contact patch. The system leveraged Epipolar geometry which allows one to determine the position of a set of matching pixels in an image pair in a global coordinate system if the geometry of the image focal planes are known. Guthrie et al. (2017) proved that outside of the tyre the system was capable of errors in the order of 2mm, and when mounted and calibrated the system was capable of producing a point-cloud of $200mm$x$280mm$ large which amounted to a $40°$ arc of a 235/85R16 tyre. Discrete obstacles could clearly be seen in the point clouds as the tyre rolled over them. The system is shown in Figure 2.1.

The system was further refined by Feldesi et al. (2020) in order to facilitate the measurement of strain with T2Cam in addition to deformation. The side-by-side camera arrangement was replaced with opposing cameras, which improved the depth resolution of the system and to an extent occlusion. A new strobing lighting arrangement was also implemented to reduce the power dissipation which would otherwise heat the tyre significantly. A Constant-Strain Triangle (CST) is used to determine the planar local strain $(\epsilon_x, \epsilon_y, \gamma_{xy})$ in the centroid of a triangle defined by three points, where the deformation of each point is relative to an undeformed reference point cloud obtained from the inflated but unloaded tyre. The strain at each point cloud

measurement is found by forming four CST's surrounding the point of interest, and averaging each strain component. Feldesi et al. (2020) validated this method with artificially strained printed images, finding that the system was accurate to within a noise band of 0.5% strain. A large-lug agricultural type Trelleborg TM700 tyre was mounted to the system for testing since the stiff lugs and minimal steel reinforcements were expected to cause high strains on the inner surface of the tyre during testing. Even when unloaded but inflated, the measured strain variation clearly showed indications of the areas where the tread blocks were present. Feldesi et al. (2020) conducted tests on the Static Tyre Test Rig (STTR) at the University of Pretoria where the tyre was loaded against a flat steel plate and the force-deflection characteristics were measured using a Wheel Force Transducer (WFT), as well as lateral and longitudinal force-displacement at various loads. A linear relationship could be found between the maximum longitudinal strain versus the vertical force, and the maximum lateral strain versus the lateral force.

Pegram et al. (2021) continued this work to improve the triggering mechanism, include the effect of slip angle, and validate the measured strain against strain gauges statically and in the rolling condition. Feldesi et al. (2020) found that peak strains occur near the edges of the contact patch, and it was chosen to place strain gauges at three locations along the length of a lug on the inside surface of the tyre close to the sidewall. At each location the strain gauges were placed in a half-bridge arrangement with two strain gauges orthogonal to each other, resulting in a measurement which is temperature compensated and can measure longitudinal or lateral strain (relative to the orientation of the strain gauges) as long as the Poisson's ratio is known. A drum type tyre test rig was used to spin the tyre under load and vary slip angle ($-5^\circ \leq \alpha \leq 5^\circ$), but was not suitable to test the tyre near its Load Index (LI). A rotary encoder was used to ensure that the strain gauges and cameras were triggered at the same time and that measurements could be compared reliably. The results of the drum tests showed that the trends in the lateral and longitudinal strain through the contact patch are similar to those one would expect if a passenger tyre was used. Pegram et al. (2021) identified that the characteristic tension and compression peaks could be used to identify parameters such as slip angle or vertical load. Pegram et al. (2021) showed that there is a strong linear relationship between the tension and both compression peaks and vertical load for the longitudinal strain, while the same variation in vertical load had a more complex relationship with the tension and compression peaks of the lateral strain. The effect of inflation pressure was seen to also have

a similar effect where the peak tension or compression in both the longitudinal and lateral strain increased as the inflation pressure dropped. The peaks in the lateral strain had a clear linear relationship with the slip angle. The strain gauge point-strain measurements were also compared to the corresponding regions of the full-field T2Cam strain measurement. It was found that the point strain measurements correlated well with the measurements from T2Cam.

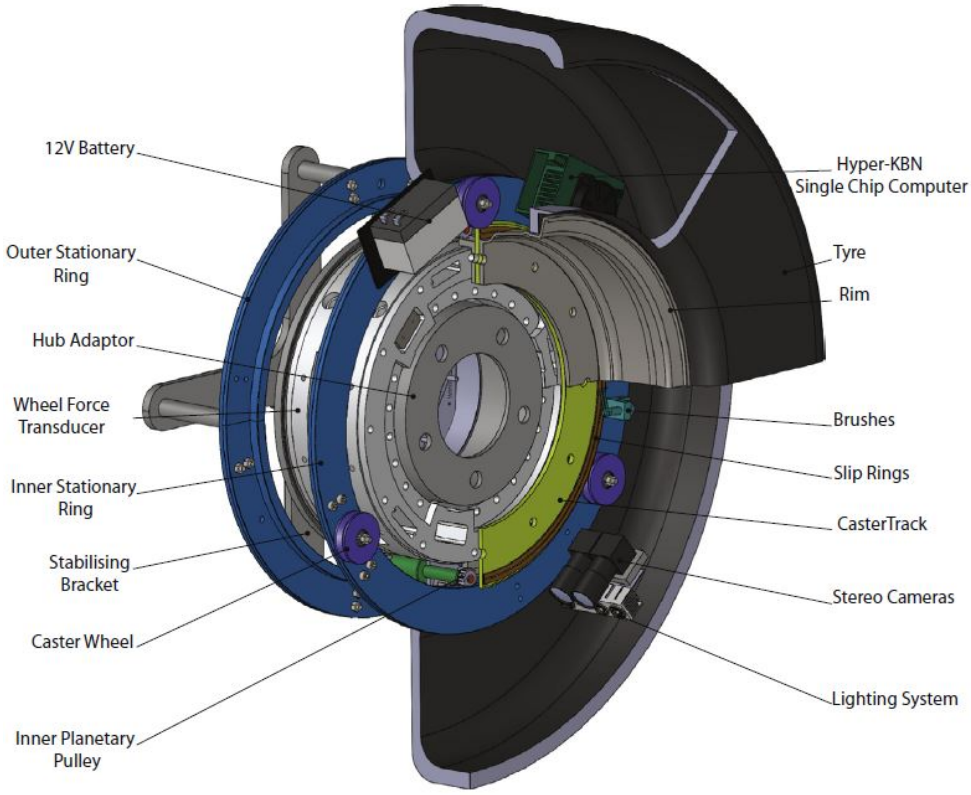

Figure 2.1: Labelled schematic of T2Cam - adapted from Guthrie (2016)

The T2Cam system is therefore able to provide reliable full-field 3D deformation and strain measurements on the inside of a rolling tyre and has extensive potential to be used in a smart/intelligent tyre application.

2.3 Tyre Models for Intelligent Tyre Concepts

Research into tyre models has occurred for nearly 100 years. For the vehicle dynamics perspective, these modelling efforts have typically centered around estimating vertical, longitudinal, and lateral force from vertical displacement, % slip, and slip angle. To date there is a wealth of knowledge on this topic as well as many survey papers and books discussing the various methods and their relative performance (Chang et al., 2004; Pacejka, 2005; Li et al., 2014; Khaleghian et al., 2017). These range from basic semi-empirical approaches like the Magic Formula (Pacejka and Bakker, 1992) and TMEasy (Hirschberg et al., 2007) to high fidelity lumped-mass and Finite Element approaches such as FTire (Gipser, 2007) and CDTire (Gallrein and Bäcker, 2007). However, there is an emerging need for a new type of tyre model which focuses on estimating the distribution of tyre forces from parameters that can be measured directly on the tyre - such as acceleration, deformation or strain on the inner surface of the tyre carcass.

There are many different methods that one can use to infer tyre parameters from sensors in an intelligent tyre. We can categorize these models as either empirical, semi-empirical, physical, or other. Empirical (or phenomenological) models are based on observation without being derived from first-principles, and therefore they can not accommodate for unexpected or new scenarios. Semi-empirical methods go one step further to model a phenomena based on some aspect of the relevant physics, but are simplified in some way or another and as such require correction factors. Semi-empirical models can sometimes operate outside of their intended domain, but can have unpredictable consequences in the model behaviour. Physical models are generally complex attempts to capture almost all of the physics of a system, but typically have dozens of parameters and are slow to solve. Physical models have a distinct advantage in that they can be used to learn new behaviour of a system - this is discussed by Gipser (2016) in reference to *FTire*. Other methods in this context encompasses Fuzzy Logic, Neural Networks, and any other method that can be broadly described as models which are not specific to the problem being solved but rather arrive at accurate prediction as a result of being extremely flexible.

Table 2.1 shows a summary of journal papers, conference proceedings, and projects in which tyre force is estimated, the type of sensor used, the tyre parameters estimated, the estimation method, and whether or not validation was performed. While is it clear that strain gauges are the most used sensor, there does not appear to be much agreement between researchers as to the best method to use this data. Earlier work relied mostly on more traditional semi-empirical

or physical methods (The European Commission, 2008; Tuononen, 2009; Matsuzaki et al., 2010; Oertel and Hempel, 2014; Yang et al., 2015) whilst the most recent work has shifted to Neural Network and Fuzzy logic approaches (Khaleghian et al., 2019; Mendoza-Petit et al., 2020; Xu et al., 2020). The lack of consensus among researchers on the modelling approach points to a lack of understanding of the relationship between the tyre-road interaction and the resulting behaviour of the tyre. Regardless of the sensor type used by an intelligent tyre, the input-output relationship is unknown and high-dimensional and this makes it difficult to propose models to recover the distribution of forces.

There is promise in semi-empirical and physical modelling approaches. Oertel and Hempel (2014) presented a modification of his existing tyre model RMOD-K FEM (Comfort and Durability Tire) (Oertel and Fandre, 2009) using simulated ''embedded measurement fibers" to virtually re-create strain gauge measurements. Oertel and Hempel (2014) demonstrated that existing FEM-based tyre models, and RMOD-K FEM in particular, are suitable for estimating tyre force via intelligent tyre but some pattern matching was required.

Holtschulze et al. (2005) presented a semi-empirical method, based on geometry, which could be used to determine the lateral force, longitudinal force, and aligning moment. This method relied on assuming the size and shape of the ground pressure distribution under the contact patch, and could not be used to infer the tyre load nor could it accommodate rough terrain. However, the model shows promise since the correlation between experiment and prediction is good. This model would solve rather fast since closed form solutions are derived, and might show promise as a means to speed up a high-fidelity physical tyre model once the vertical force is known.

Matsuzaki et al. (2010) proposed a very simple model based on integrating the circumferential strain, although it appears that this method is intended for strain gauges embedded in the tyre carcass. Matsuzaki et al. (2010) obtains the vertical force by integrating the 'vertical' strain from the beginning of the contact patch to the end. The circumferential (measured) strain is defined as the summation of the frictional strain and the vertical strain, where the frictional strain is the derivative of the circumferential deformation due to friction with respect to the contact patch. To estimate the longitudinal force Matsuzaki et al. (2010) assumes a particular form of the frictional and circumferential strains, and applies a similar procedure of

Table 2.1: Summary of tyre force-predicting intelligent tyre concepts

Year	Author(s)/Project	Sensor	Tyre Parameter(s)	Method	Validated?
2008	FRICTI@N	Optical	F_y F_x F_z	Semi-Empirical	Yes Yes Yes
2009	Tuononen (2009)	Optical	F_y F_x F_z	Empirical	Yes Yes Yes
2010	Matsuzaki et al. (2010)	Strain Gauge	F_z F_x	Physical	Yes (FEM) Yes (FEM)
2014	Oertel and Hempel (2014)	Strain Gauge	F_x F_y F_z	Physical	No No No
2015	Yang et al. (2015)	Strain Gauge	F_x F_y F_z	Physical	Yes Yes Yes
2016	Khaleghian et al. (2016)	Accelerometer	Contact Length F_z	Neural Network	Yes Yes
2017	Garcia-Pozuelo et al. (2017a)	Strain Gauge	F_z Angular Velocity	Fuzzy Logic	Yes Yes
2017	Garcia-Pozuelo et al. (2017b)	Strain Gauge	F_z α	Fuzzy Logic	Yes Yes
2018	Yunta et al. (2018)	Strain Gauge	F_y F_z α	Empirical Fuzzy Logic	Yes Yes Yes
2018	Feldesi et al. (2020)	Optical	F_y F_z	Empirical	Yes Yes
2019	Garcia-Pozuelo et al. (2019b)	Laser	Strain Profile	Semi-Empirical	Yes
2019	Lee and Taheri (2019)	Strain Gauge	F_z Contact Length	Semi-Empirical	Yes Yes
2019	Garcia-Pozuelo et al. (2019a)	Strain Gauge	F_z	Semi-Empirical	Yes
2019	Khaleghian et al. (2019)	Accelerometer	F_y F_x F_z	Neural Network	Yes Yes Yes
2020	Mendoza-Petit et al. (2020)	Strain Gauge	Rolling Radius Contact Length	Fuzzy Logic	No No
2020	Xu et al. (2020)	Accelerometer	F_y F_x F_z	Neural Network	Yes Yes Yes

integrating the frictional strain across the contact patch. Clearly this method assumes that there is negligible variation in the strain measured compared to the strain at the contact patch of the tyre, which may not always be accurate. In fact, when compared to experimental measurement Matsuzaki et al. (2010) shows that the model can predict vertical force well, but if the 'frictional load' is varied then the accuracy decreases by around 20%. A similar trend is seen in the predicted vs. experimental frictional load, where variations in the applied load to the tyre causes inaccuracies especially at higher frictional loads. This behavior highlights the main disadvantage of simple semi-empirical models.

Garcia-Pozuelo et al. (2019a) presented a real-time model to accurately predict the strain profile of a rolling tyre on flat, rigid terrain. A Flexible Ring Tyre Model (FRTM) formed the basis of the model, where the 6^{th} order partial differential equations of motion of the discretized treadband was adapted into a closed form solution for the circumferential treadband strain using the Modal Expansion Method (MEM) - this has the benefit that the calculation can be performed quickly. The model is characterized as semi-empirical and therefore few parameters need to be fitted. The model was validated for various inflation pressures, loads, and longitudinal forces against experimental data. One could likely solve this problem in the inverse fashion to determine the vertical and longitudinal force given the measured strain profile. We can compare this work to that of Yang et al. (2015) where the same intelligent tyre concept was used, except a 3D FEM model of the tyre was used to predict all three tyre forces. In this case the correlation between prediction and experiment was excellent, and more importantly this method is much less sensitive to parameter variations - i.e. if one is to predict lateral force with this method, then variations in inflation pressure or load do not appear to have a significant effect on the accuracy of the model. The work by Yang et al. (2015) makes it clear that a high-fidelity physical model, such as a FEM model, can be invaluable in developing a model for an intelligent tyre since they allow one to quickly and cheaply produce a large dataset of virtual experiments. One can tightly control the loading scenarios of these virtual experiments such that the true external forces are exactly known, and there are no measurement errors.

The work done by Garcia-Pozuelo et al. (2017a,b) focused on applying Fuzzy Logic to predict tyre force from strain measurements, which proved to be very accurate. Hundreds of 'if-then' rules are used to estimate the outputs, but this approach has parameters which are not physically significant. This approach also has the disadvantage that the model complexity

grows exponentially with each new input, and the designer must pre-program the range of inputs that can be handled - in this way the method is not flexible to unexpected inputs from new environments.

2.4 The Tyre Studied

To simplify the problem a tyre is investigated which does not have steel bands running from bead-to-bead and, therefore, will have macroscopic material properties closer to rubber. Additionally, the effects of tread block deformations are removed by choosing a slick tyre with no tread blocks. The tyre being studied is a Trelleborg TM700 280/70R16 agricultural tyre (Figure 2.2a), the same tyre used by Pegram et al. (2021) except with the tread lugs shaven off. This tyre does not have steel cords running from bead-to-bead and is, therefore, suitable for the analysis. The tyre geometry has already been captured with a combination of profile gauges and laser scanning and converted into a Computer-Aided Design (CAD) model for previous studies. A cross-sectional view of the shaved tyre in CAD is shown in Figure 2.2b.

2.5 Axis System

The description of forces and moments transferred to or from a tyre requires defining an appropriate axis system. For the investigation of tyre behaviour, an axis system that is centred around the tyre is preferred. For this study, the TYDEX (TYre Data EXchange Format) C-axis system is adopted as shown in Figure 2.3. In the TYDEX C-axis system, the x-axis is defined as the line in the wheel plane parallel to the ground plane. The y-axis is perpendicular to the

(a) A Trelleborg TM700 with the tread lugs removed

(b) TM700 CAD cross-section with the tread lugs shaven off

Figure 2.2: CAD geometry of the shaved tyre

wheel plane and therefore is the spin axis, and the z-axis follows from the right-hand rule. The slip angle is the included angle between the tyre heading and the direction of travel. The tyre inclination, or camber angle, is also shown. This is the angle between the ground plane normal and the tyre spin axis normal.

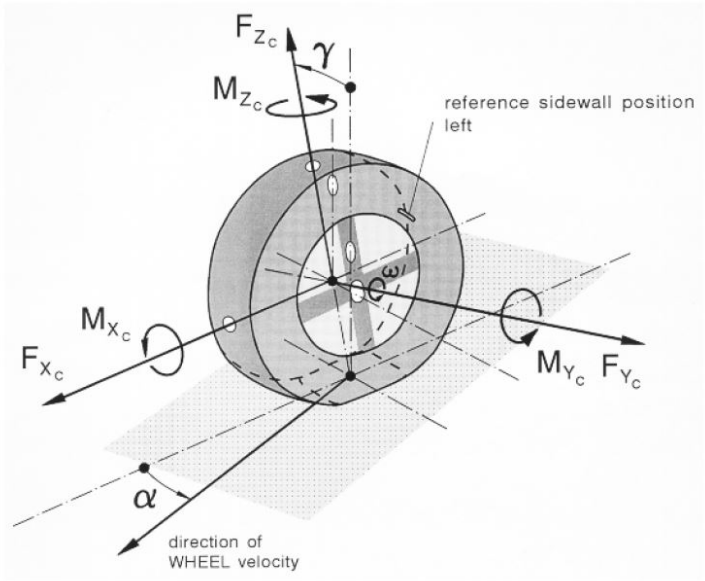

Figure 2.3: TYDEX C tyre axis system - adapted from Van Oosten et al. (1997)

2.6 Chapter Summary

Tyre modelling efforts catering for intelligent tyre concepts are rapidly evolving, with most of the development in the 21st century occurring in the last 2-3 years. The current state-of-the-art in intelligent tyre models is limited to predictions of total forces from a single measurement, and these methods should be extended to be able to predict the distribution of external forces from a full-field measurement from an intelligent tyre such as T2Cam. Empirical methods show promise for real-time estimation but are generally quite limited in their application, where much of the available work is for smooth terrain. Semi-empirical methods show even more promise, and in some cases can be used in real-time, but still generally have a narrow domain of application. Other methods like Fuzzy Logic and Neural Networks should not be ignored as they too have potential to handle a wide range of scenarios, but grow in complexity exponentially as inputs are added. The physical models show the most promise, specifically the FEM-based methods, as they can be used in the most scenarios however they have the drawback that the solution time is long. Most importantly a finite element model will naturally involve the distribution of external forces, which is the ultimate research goal. Since physical methods allow for a close approximation of the true physics one can produce large amounts of virtual test data for developing a model to identify tyre forces from internal deformations and strains.

Chapter 3

Tyre Model Development

3.1 Overview

In this thesis the identifiability of external forces on a tyre from internal measurements will be studied, and as there is little evidence in literature to suggest the uniqueness of a solution it is wise to make use of a model which captures the essential physics of the problem. For this reason, a Finite Element Method (FEM) model of the tyre being investigated will be developed as this allows one to approximate the full deformation field of a tyre. In this chapter the development of two FEM models for this purpose is described, one where the full tyre geometry with inflation effects is present and one where an un-inflated partial section of a tyre with reduced geometry is used. The models are meshed using the open-source finite element mesh generator Gmsh (Geuzaine and Remacle, 2009) as it allows for very fine, manual control of the mesh. The models themselves are modelled in the open-source finite element analysis application CalculiX (Guido Dhondt, Klaus Wittig, 1998). CalculiX is lightweight, well featured, and runs on ABAQUS input and output files. Therefore, it is easy to write scripts to generate input files, evaluate them with CalculiX, and retrieve the results. This makes CalculiX a perfect tool for the optimisation-based study presented in Chapter 4.

3.2 Tyre Model Description

The reduced geometry model is modelled as the bottom 90° section of the tyre which is adjacent to the road surface, which is just large enough such that at the most extreme virtual experiment

the contact patch is less than half the total width of the geometry. The mesh of the tyre is generated with the open-source tool Gmsh (Geuzaine and Remacle, 2009) with incompatible mode eight-node brick elements (C3D8I) to facilitate using a non-linear hyperelastic material model, with 440 elements and 880 elements for the reduced geometry and full tyre respectively. A slightly coarser mesh is used for the full tyre so as to reduce computational effort, hence it has 880 elements and not four times that of the reduced geometry model. The material for both models is modelled as Neo-Hookean. The equivalent Young's Modulus and Poisson's ratio ν for each model is shown in Table 3.1. For the reduced geometry model the material was chosen to be on the low end of the scale of typical rubber stiffness's found in tyres, as it is expected that it will better expose the sensitivity of the problem. The radial cords embedded in a tyre's carcass increases the stiffness of the tyre in the direction that the cords run and is typically modelled in FEM with orthotropic elements - adding effort to determine additional material properties. This orthotropic behaviour is instead modelled by having standard isotropic material properties for all elements but (manually) varying the material properties to recreate the macroscopic behaviour of the tyre, which ensures that the overall stiffness can be matched even if the elements themselves do not accurately reflect the local behaviour of a tyre. The equivalent Young's Modulus of the tread, bead, and sidewall regions are each independently varied until the vertical stiffness of the tyre matches that of a laboratory experiment. The final material properties, shown in Table 3.1, are still representative of real material properties found in previous studies (Stallmann et al., 2014; Conradie et al., 2016). However, even if these numerical material parameter values turn out to be unrealistic, the study remains valid. The goal is to determine if the external tyre forces are identifiable from internal displacement and strain measurements.

The boundary conditions at the bead are modelled as a fixed displacement, which has been shown to have a negligible effect on the tyre's vertical stiffness compared to a full contact simulation of the rim-bead interaction Stallmann and Els (2014). The boundary condition between the tyre and the flat, smooth road is iteratively applied by first displacing the node on the tread which most violates the road for a given total displacement, running this simulation to determine the new penetration with the road, and then repeating this process until no tread nodes penetrate the road. If a node presents an opposing reaction force in the z-direction at any stage (tensile reaction force instead of compressive), it is released. For the full geometry virtual experiments this boundary condition is replaced by hard contact with a flat plane of nodes which represent the road surface for a particular loading condition, where the penalty for

		Model Type	
		Reduced Geometry	Full Geometry
Road Boundary Condition		Iterative Procedure	Hard Contact, Exponential Penalty
Internal Pressure		No	Yes
Young's Modulus	Tread	10 MPa	60 MPa
	Sidewall	10 MPa	20 MPa
	Bead	10 MPa	20 MPa
Poisson's Ratio		0.499	0.4
Number of Elements		440	880

Table 3.1: Summary of differences between the two FEM tyre models developed

contact violations is exponential and was determined by iterating through parameters until the penetration between tyre and road was negligible for a tyre inflated to 2 bar and subjected to a deformation of 30mm. These simulations allows one to determine the strains and displacements inside the tyre, given some loading, representing what one can measure in the laboratory on an actual tyre. The differences between the reduced and full geometry models are summarised in Table 3.1.

3.3 Virtual Experiments

An inverse problem is being solved in this study, and Virtual Experiments can be used to better understand the behaviour of this inverse problem. The inputs and outputs of a Virtual Experiment can be tightly controlled and therefore there is no uncertainty in whether or not the inverse method finds the true answer (Wilke et al., 2010; Asaadi et al., 2017; Ben Turkia et al., 2019). One first generates a virtual experiment for a given loading condition which returns stresses, strains, deformations, and forces. The strains and deformations on the inside of the tyre are considered to be the "measurements" from the virtual experiment, while the forces on the outside of the tyre is the solution to be recovered. Virtual experiments are generated for various scenarios for both the full and reduced geometry models, where the only variable in the reduced geometry model is the total displacement while the full geometry model also adds inflation pressure. Virtual experiments are used in place of real measurements from T2Cam. If the proposed methods do not work with ideal virtual measurements, they are unlikely to work on noisy measurements from T2Cam. In Sections 3.3.1 and 3.3.2 an example of a typical virtual experiment for each model is presented.

3.3.1 Reduced Geometry Model

Figure 3.1 shows various results of a virtual experiment in which the test section was displaced by 30mm, which corresponds to typical displacements that the tyre might sustain under heavy loads. Figures 3.1a and 3.1c indicate that in the absence of inflation pressure, the test section bulges in the middle, causing a loss of contact in the centre of the test section. This bulging phenomenon is expected behaviour, and can be readily replicated experimentally if desired. The reaction forces at the tyre tread resulting from the displacement are shown in Figure 3.1b, where the total vertical reaction force was 359N spread across two distinct areas of contact. The average nodal force over these nodes in contact is 25.68N with a standard deviation of 7.27N. Figures 3.1d, 3.1e and 3.1f show the three components of percentage surface strain calculated from the full-field displacement measurements. These indicate how rapidly the strain dissipates from the inside of the tyre to the outside of the tyre.

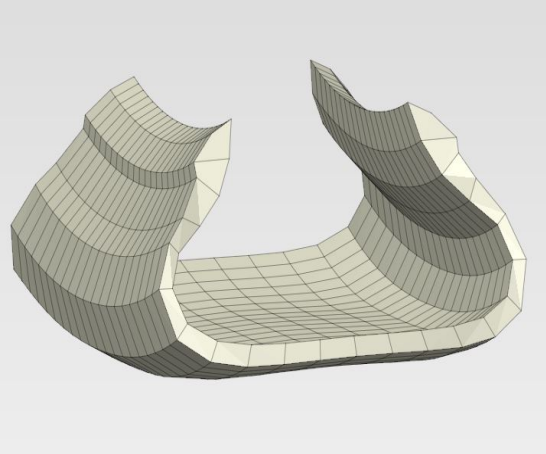

(a) Deformed geometry

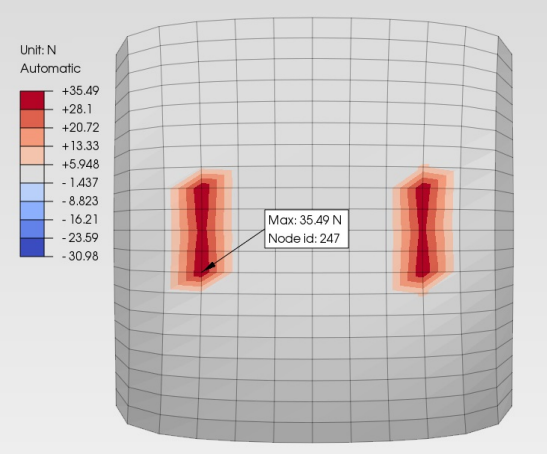

(b) Vertical reaction forces, bottom view

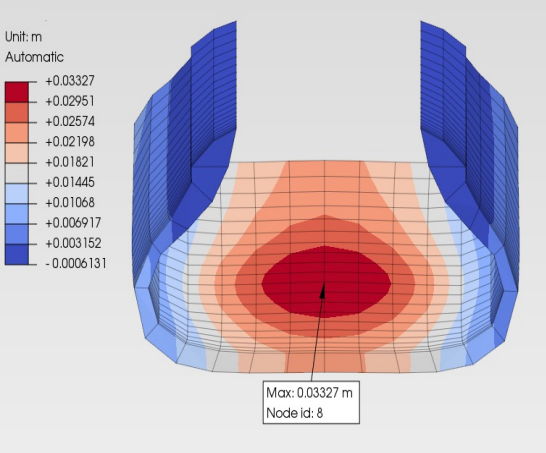

(c) Vertical deformation

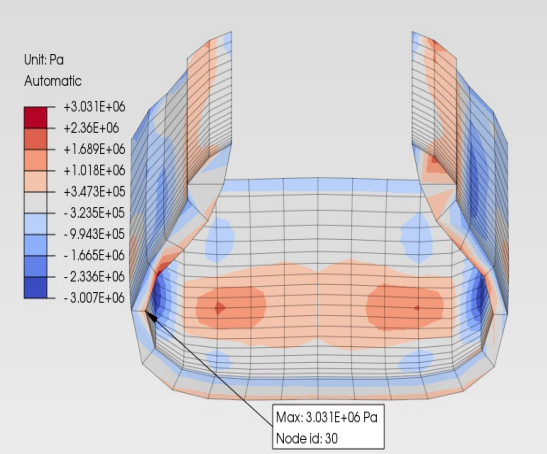

(d) ϵ_{xx}

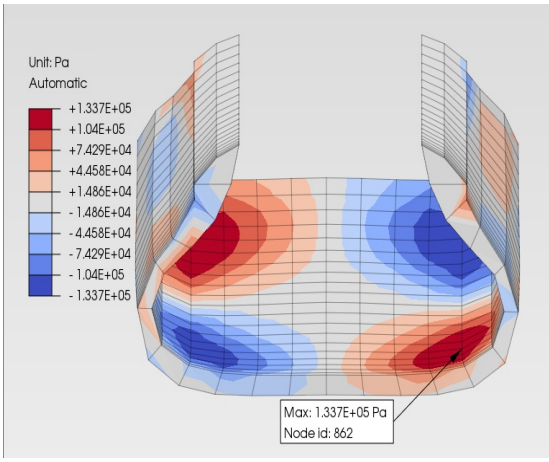

(e) ϵ_{xy}

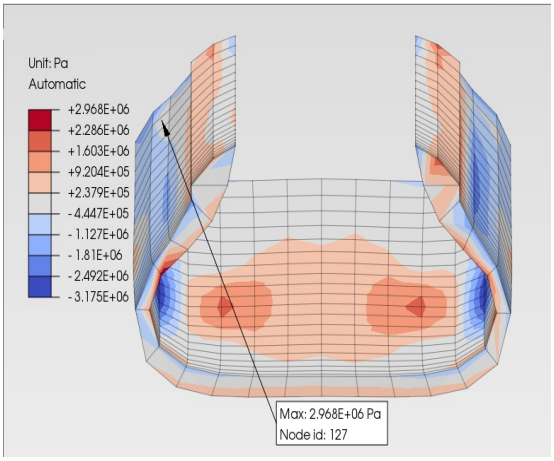

(f) ϵ_{yy}

Figure 3.1: Results from a reduced geometry virtual experiment for a 30mm displacement

3.3.2 Full Geometry Model

The results of a typical virtual experiment for a full tyre are shown in Figure 3.2 where the displacement is 30mm and the tyre is inflated to 80kPa. Experiments have already been conducted at 80kPa and 200kPa for the tyre that this study is based on (Becker and Els, 2022), and as such these pressures will be used for the investigations that follow. From the cross-section of the tyre shown in Figure 3.2a it is clear that the section that is in contact with the road appears similar to the virtual experiment in Section 3.3.1 but the bottom of the tyre is flat against the road, which is due to the inflation pressure which prevents the bulging phenomenon. The inflation pressure places the tyre in a state of tension which is exaggerated in this case due to the omission of any kind of reinforcing fibres in the material model, which causes the tread of the tyre to bulge out more than expected. The bulging due to pressure on the real tyre is at most 4mm at 200kPa while the corresponding virtual experiment bulges by 8mm. If the tread is not modelled as being stiffer than the sidewall and bead then this bulging can increase to 16mm or more. This bulging will later be shown to have negligible effects on the macroscopic stiffness of the tyre in the direction of interest in Section 3.4. The vertical reaction forces produced by the loading are concentrated in a region at the center of the contact patch of the tyre, shown in Figure 3.2b, where the total force was 4475.5N with an average nodal force of 263.3N and standard deviation of 227.4N. The vertical deformation of the inside of the tyre is shown in Figure 3.2c which has a similar shape to that of Figure 3.1c, except the vertical deformation does not exceed 30mm. The three components of percentage surface strain calculated from the full-field displacement measurements are shown in Figures 3.2d, 3.2e and 3.2f. The lateral and shear strain components present similar patterns to those in Section 3.3.1, but there is significantly less variance in the longitudinal strain. This is due to the inflation pressure which causes such high tension in the tread of the tyre that the loading does not cause the strain to become compressive in the vicinity of where the external loading is applied. This effect has a similar but less prominent effect on the lateral strain, but it is still clear that the strain in Figure 3.2f is more uniform than in Figure 3.1f.

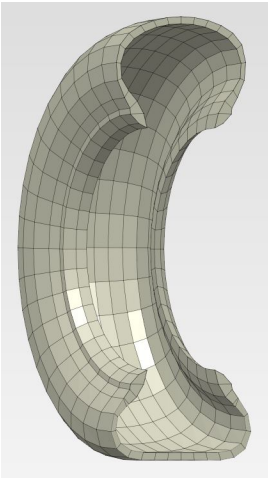

(a) Deformed geometry

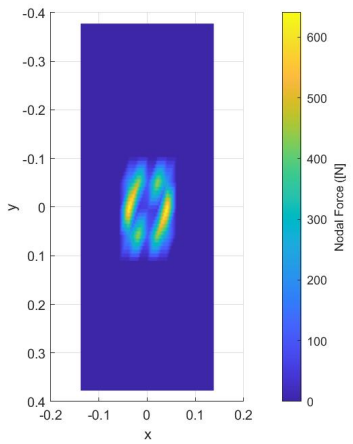

(b) Vertical reaction forces, bottom view

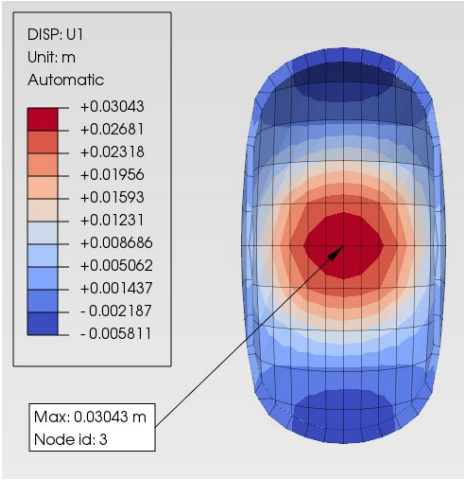

(c) Vertical deformation

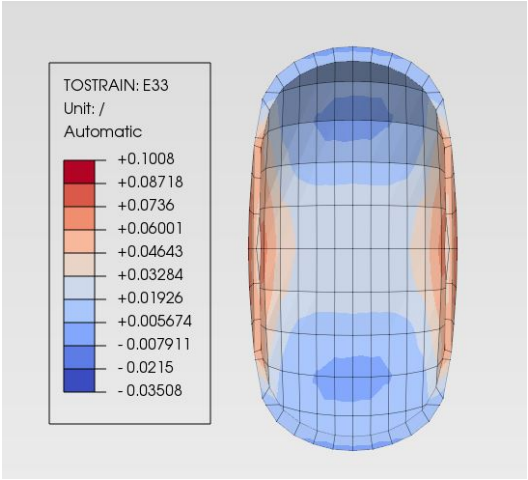

(d) ϵ_{xx}

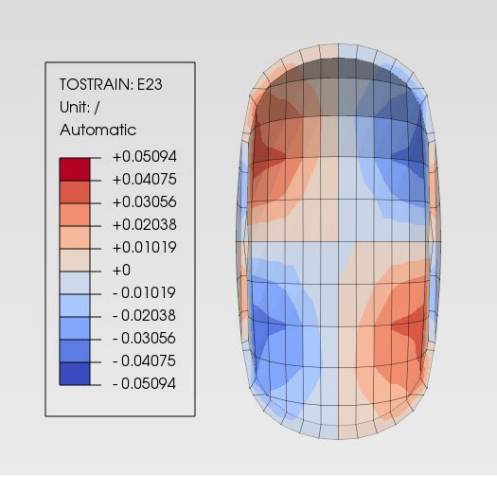

(e) ϵ_{xy}

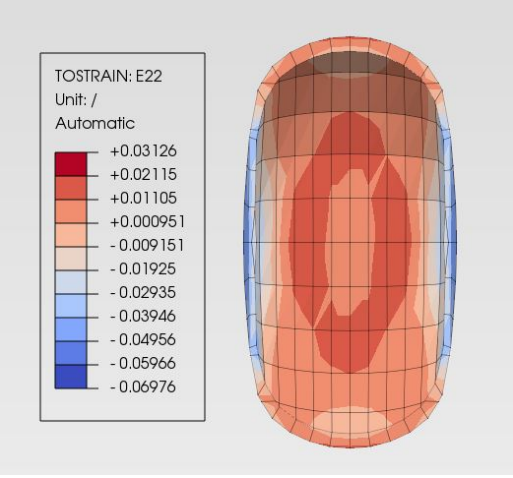

(f) ϵ_{yy}

Figure 3.2: Results from a full geometry virtual experiment for a 30mm displacement inflated to 80kPa

3.4 Validation

The two models presented offer a physical description of the physics which govern the deformation of a tyre subject to some loading. Since this study is aimed at understanding the overall identifiability of tyre forces from measurements, the models need not perfectly represent all the local behaviours of the real tyre so long as those local behaviours are "tyre-like" as discussed in Sections 3.3.1 and 3.3.2. If the models can replicate the overall macroscopic behaviour of a real tyre, then one can assume that the local behaviours should be representative even if they might not be exact. In this section it is shown that the full geometry model presents good correlation of its vertical stiffness versus vertical deflection characteristics when compared to the tyre it was modelled after. This comparison is not made for the reduced geometry model as it would require some special equipment to reproduce the boundary conditions enforced in FEM.

Figure 3.3 shows the vertical force versus vertical displacement curves for a Trelleborg TM700 with the tread lugs shaven off as acquired by Becker and Els (2022). In this test the tyre was inflated and then subsequently pressed against a smooth steel plate on a large tyre testing rig, where displacements were applied slowly so as to approximate a quasi-static loading condition. Two datasets were recorded for inflation pressures of 80kPa and 200kPa. Figure 3.3 also shows the force-displacement predictions from the full geometry model for the same pressures, except in FEM only 9 data points are recorded for each pressure (from 0mm to 40mm displacement). There was no friction enabled in FEM so the boundary conditions between the simulation and experiment are not the same, however Becker and Els (2022) shows that friction has very little influence over the vertical characteristics. As such one can assume that the virtual experiment still closely resembles a real experiment where there is no friction between the tyre and the steel plate. The simulation and experiment agree well given that the model used is coarse and does not model the individual fibres and the rubber and steel regions in the tyre. The experiment shows that the stiffness of the TM700 tyre depends on displacement, and this effect is more prominent for higher inflation pressures. The tyre stiffening due to displacement is approximated well by the model. The tyre becomes more stiff as the pressure increases which is also captured by the model. The RMS error for the 80kPa and 200kPa simulations is 107.32N and 215.18N respectively. The mean stiffness of the 80kPa and 200kPa simulations was 0.81kN/m and 1.46 kN/m compared to a mean stiffness of 0.99kN/m and 1.62kN/m for the experiments. The plot of the normalized (relative to the corresponding experimental data

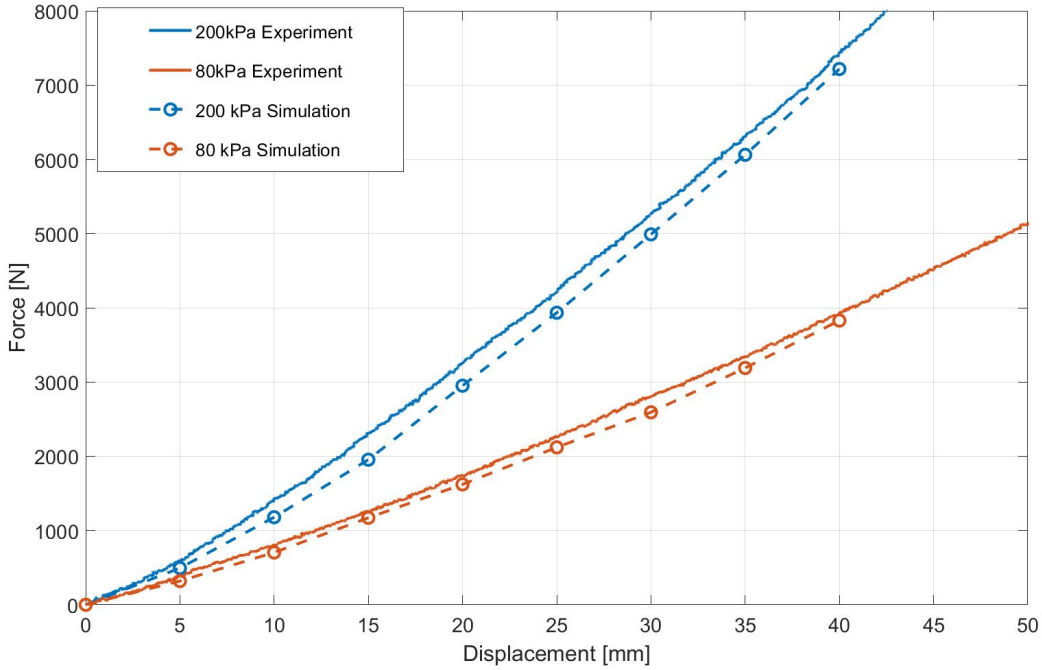

Figure 3.3: Predicted and experimental force-displacement curves of the Trelleborg TM700

at each total displacement) and un-normalized error versus displacement for both pressures is shown in Figure 3.4 and shows that although normalized errors are large when the force predicted is small, there is a trend towards a normalized error of below 0.2 for more realistic displacements. The un-normalized errors reach a maximum of 262N at a 25mm displacement for an 80kPa simulation where the corresponding total force predicted was 3933N.

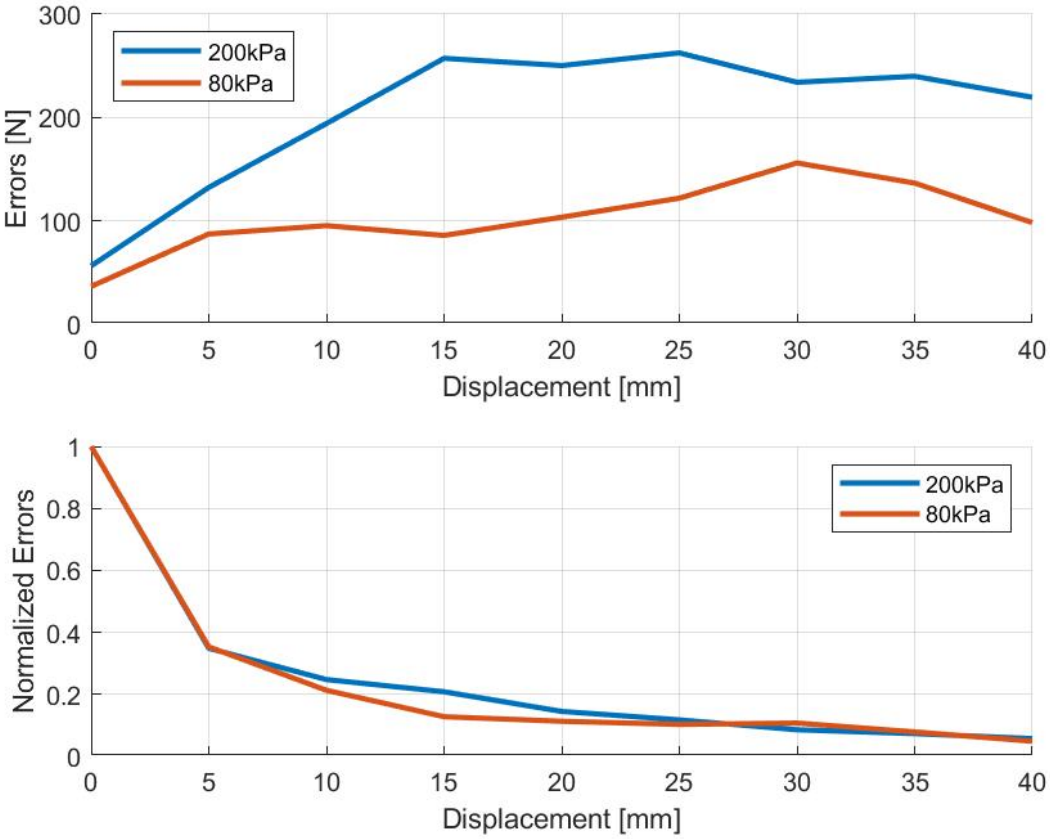

Figure 3.4: Errors and normalized errors between the experiment and simulation for the Trelleborg TM700

3.5 Chapter Summary

In this chapter two finite element models were developed in order to produce virtual experiments for the inverse analysis to follow. The reduced geometry model has simplified boundary conditions as it is theorized that this will cause excessive deformations and expose the sensitivity of the inverse problem. The reduced geometry model also reduces the dimensionality of the problem from a full 2D contact patch to just two lines of contact that must be determined from deformation or strain measurements. The full model captures the essential physics of an inflated tyre loaded against a frictionless plate. Open-source tools are used to pre-process and run the FEM code to generate virtual experiments. Typical results from virtual experiments are presented for both models, and the second model is validated against experimental results of the tyre it was modelled after. The correlation between the second model and the experiment was found to be inline with the accuracy desired for this study. This validation gives confidence in both models for the identifiability study that follows, whereby a virtual inverse problem is

solved to identify external tyre forces from strain or deformation measurements inside the tyre.

Chapter 4

Identifiability Study

4.1 Overview

In this chapter the "naive" approach of estimating the distribution of external forces is investigated. It would be desirable to recover the distribution of external forces as well as the total forces and moments acting on a tyre given some measured internal displacements and/or strains. The reduced geometry model is used for this investigation as the approach requires optimisation in a high-dimension therefore a model which is fast to compute and has simplified physics is preferred. The problem is solved by using optimisation to apply forces to individual nodes on the outside of the tyre until the resulting strains or deformations on the inside match those of a corresponding virtual experiment.

4.2 Optimisation-based Virtual Inverse Simulations

Given some measured displacement $\boldsymbol{U}$ or strain $\boldsymbol{\epsilon}$ inside the tyre, the corresponding external forces, $\boldsymbol{x}$, that caused them must be recovered. The challenge is that the forces must be recovered at a different location to where the displacements and strains are measured. An optimization-based approach is suitable for matching the strains and displacements on the inner surface of the tyre to the corresponding virtual experiment, where the input space is the distribution of external forces. An initial guess, $\boldsymbol{x}_0$, of the external forces applied to the outside of the tyre is required to solve the virtual inverse problem. The resulting displacements or strains are computed and compared to those computed in the virtual experiment. When

good agreement is found the procedure terminates, else the optimizer updates the forces and repeats the process until convergence is reached. It may be the case that the deformations and strains on the inner surface of the tyre actually contain different information about the forces that caused them, and as such they are investigated as two different cost functions to identify the distribution of forces. In practice it may be beneficial to use both strain and deformation in a more sophisticated cost function to identify the distribution of forces. The locations at which forces can be applied are restricted to those where contact does occur to reduce the dimensionality of the problem from 225 unknowns (all possible tread nodes on the tyre) to 14. The unconstrained Nelder-Mead optimization algorithm is used to solve the optimization problems

$$\underset{\boldsymbol{x}}{\text{minimize}}\, f(\boldsymbol{x}) = \sqrt{\frac{\sum (U_x - U_x^*(\boldsymbol{x}))^2 + \sum (U_y - U_y^*(\boldsymbol{x}))^2 + \sum (U_z - U_z^*(\boldsymbol{x}))^2}{N}}, \text{ and} \quad (4.1)$$

$$\underset{\boldsymbol{x}}{\text{minimize}}\, f(\boldsymbol{x}) = \sqrt{\frac{\sum (\widetilde{\epsilon_{xx}} - \widetilde{\epsilon_{xx}^*}(\boldsymbol{x}))^2 + \sum (\widetilde{\epsilon_{yy}} - \widetilde{\epsilon_{yy}^*}(\boldsymbol{x}))^2 + \sum (\widetilde{\epsilon_{xy}} - \widetilde{\epsilon_{xy}}^*(\boldsymbol{x}))^2}{M}} \quad (4.2)$$

where $\boldsymbol{U}$ and $\boldsymbol{\epsilon}$ are the vectors of N nodal displacements (U_x, U_y, U_z) and M nodal strains $(\widetilde{\epsilon_{xx}}, \widetilde{\epsilon_{yy}}, \widetilde{\epsilon_{xy}})$ on the inner surface of the test section from the virtual experiment, while $\boldsymbol{U}^*(\boldsymbol{x})$ and $\boldsymbol{\epsilon}^*(\boldsymbol{x})$ are the N nodal displacements and M nodal strains $(\widetilde{\epsilon_{xx}}(\boldsymbol{x}), \widetilde{\epsilon_{yy}}(\boldsymbol{x}), \widetilde{\epsilon_{xy}}(\boldsymbol{x}))$ on the inner surface of the current iteration of the virtual inverse problem. The nodal strains $((\widetilde{\epsilon_{xx}}, \widetilde{\epsilon_{yy}}, \widetilde{\epsilon_{xy}}),\ (\widetilde{\epsilon_{xx}}(\boldsymbol{x}), \widetilde{\epsilon_{yy}}(\boldsymbol{x}), \widetilde{\epsilon_{xy}}(\boldsymbol{x})))$ are extrapolated from the strains at the integration points of each element to the nodes on the inner surface of the tyre. This is done because T2Cam reports surface strains, while the FEM solver reports strains only at integration points inside of elements. The design vector $\boldsymbol{x}$ is the forces applied to the outside of the test section, and $f(\boldsymbol{x})$ is the objective function used in the optimization. Equations 4.1 and 4.2 are displacement-based and strain-based virtual inverse problems treated as different methods in this study but can be combined into one objective function for a third formulation.

If two distinct force distributions produce the same total force and same moments, they are known as statically equivalent (Gere and Goodno, 2009). In the problem under consideration, the force distribution is symmetric, therefore M_x and M_y are both zero. Therefore, if the sum of the design vector x solved for in the virtual inverse problem approximately equals the total force acting on the tyre F_z, and the moments M_x and M_y are approximately zero, then the identified nodal loads are statically equivalent to the correct loads.

The design vector $\boldsymbol{x}$ is a distribution of force and has a particular shape, which is desirable to recover in addition to the total forces and moments. This distribution of forces recovered from the virtual inverse simulation can be compared to the virtual experiment as a distribution of errors. A distribution of errors which is zero-mean with a low standard deviation relative to the largest nodal force predicted by the virtual experiment indicates that the design vector $\boldsymbol{x}$ has a similar distribution to the true answer.

4.3 Ideal Virtual Inverse Simulations

The best-case scenario to recover forces from measured displacements or strains would occur if there is no appreciable measurement noise and the initial guess is good. Such a scenario is a useful baseline for comparisons to the inverse solutions that follow. Two virtual inverse simulations were performed, one using the displacement-based cost function and the other with the strain-based cost function. In both cases the initial guess was chosen to be 90% of the known answer from the virtual experiment and therefore has the correct shape but lower magnitude. Figure 4.1 shows the results of solving for the contact forces using both virtual inverse methods. The net force in the displacement-based cost function was 359N and 357N for the strain-based cost function. The standard deviation of the distribution of forces from the virtual experiment was 7.27N (25.68N mean), while that of the displacement-based and strain-based cost function was 7.39N (25.66N mean) and 7.37N (25.52N mean) respectively. In both cases, the objective function converged to a zero error (within the limits of machine precision), and although the distribution of the force is not perfect, it is a reasonable reflection of the expected forces. In both cases a small moment about x and y was present due to the errors in the force distribution, however, they are all under 0.9Nm. Since it is difficult to interpret the magnitude of these moments, once can model these moments as forces applied at the edge of the contact patch. From the size of the contact patch, M_x moments are statically equivalent to a force 20x larger while the M_y moments are statically equivalent to a force 10x larger. Therefore these moments can be produced by a load as large as an 18N force (5% of the total vertical force) applied at the edge of the contact patch.

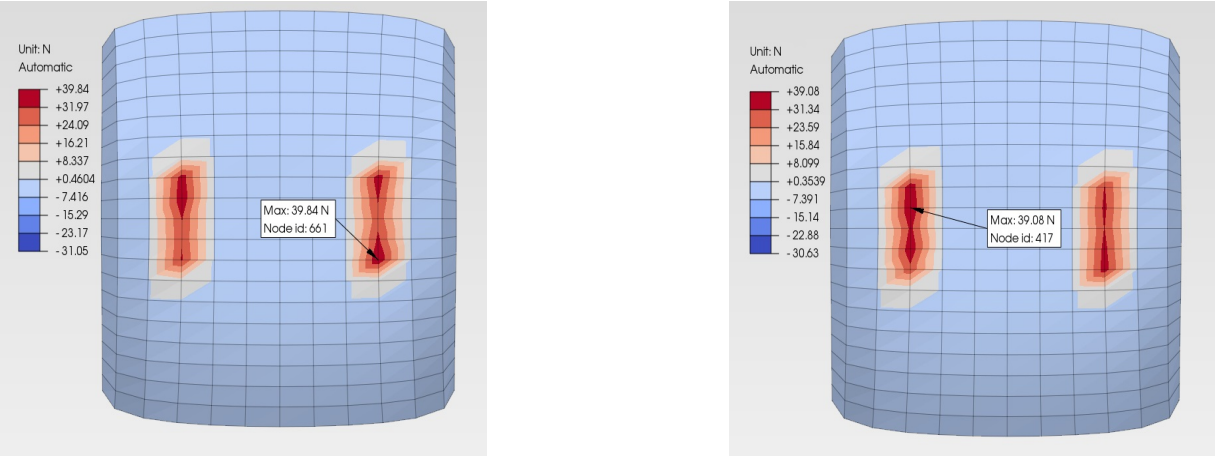

(a) Displacement-based (b) Strain-based

Figure 4.1: Identified Vertical Reaction Forces

4.4 Effects of Measurement Noise

As this study is focused on the identifiability of the forces resulting from a virtual inverse simulation, comparisons between the two methods will be made for comparable levels of uncertainty. The effect of uncertainty in the measurements was investigated by sampling from zero-mean Gaussian distributions and adding this to the virtual measurements during a virtual inverse simulation. This level of uncertainty in the displacement measurement was set to 1mm standard deviation to correspond with previous work (Feldesi et al., 2020). In order to make comparisons between the two methods, the level of artificial noise added to the deformation should be equivalent to that of the strain. This was done by ensuring that the ratio of the deformation noise level to the average nodal tread deformation was the same as the strain noise level to the average nodal tread strains, which results in a standard deviation of 0.04%. During the virtual inverse simulation the current strain or displacement is compared to a noisy version of the virtual experiment at each iteration. The initial guess remained as 90% of the known answer from the virtual experiment, as the intent of this portion of the study is aimed at understanding the effect of noise on the identifiability of external forces.

Table 4.1 shows the total vertical force and both moments (M_x, M_y) from the virtual experiment and the predictions from both virtual inverse simulations with and without measurement noise. The forces and moments for the noisy simulations were averaged over 10 runs. This level of noise does not significantly impact the forces' identifiability, since the total vertical force is predicted well, and there are negligible moments predicted where one expects zero

moments. Table 4.2 shows the RMSE in the displacement and strain inside the test section with and without additive noise. In cases where the displacement-based formulation was used, the RMSE on the strains is not significantly worse than if a strain-based method is used and vice-versa. Measuring strain fields with T2Cam requires additional post-processing on top of capturing the deformation fields, thus if the two different cost functions produce similar results it is preferred to only use deformation for an intelligent tyre model.

The force error at each node from the virtual inverse simulation to the reference force from the virtual experiment is calculated for both the strain and deformation formulations. A histogram of these errors is presented in Figure 4.2. Both distributions are zero-mean, but the displacement-based method's standard deviation was 2N whilst that of the strain-based method was 3.2N.

Table 4.1: Forces and moments predicted by virtual inverse simulations with and without noise

	F_z N	M_x Nm	M_y Nm
Reference	359.08	0	0
Displacement-based	359.23	-0.840	-0.019
Strain-based	356.71	-0.15	-0.25
Displacement-based + $\mathcal{N}(0,1)$	358.28 $\pm$0.4	-0.84 $\pm$0.1	-0.020 $\pm$0.05
Strain-based + $\mathcal{N}(0,0.04)$	357.40 $\pm$0.9	-0.2 $\pm$0.02	-0.27 $\pm$0.01

Table 4.2: Average RMSE for the virtual inverse simulations with and without measurement noise

	U_x mm	U_y mm	U_z mm	ϵ_{xx} μ	ϵ_{yy} μ	ϵ_{xy} μ
Displacement-based	0.0075	0.012	0.049	116.60	172.07	138.53
Strain-based	0.030	0.19	0.24	485.70	560.16	252.52
Displacement-based + $\mathcal{N}(0,1)$	0.010	0.040	0.070	131.08	171.22	147.54
Strain-based + $\mathcal{N}(0,0.04)$	0.27	1.93	2.25	4538.7	5089.14	2530.81

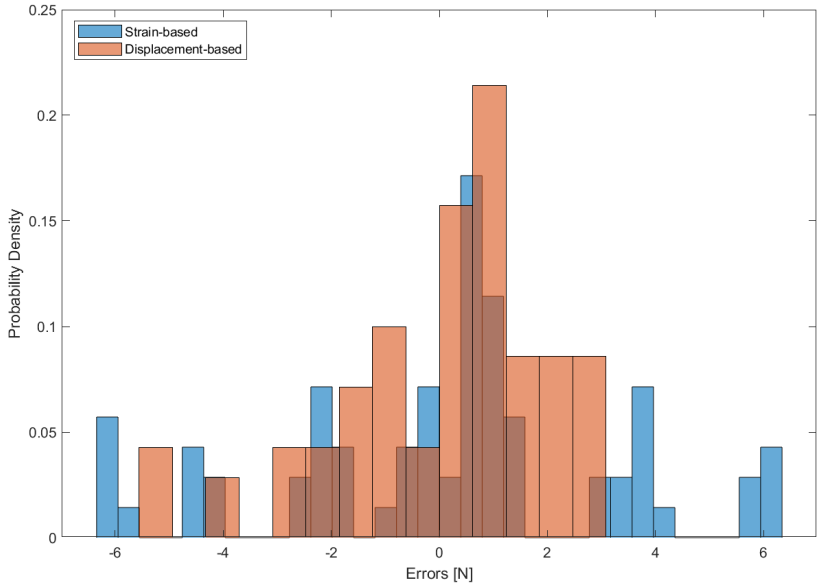

Figure 4.2: Spread of the normalized errors on the forces recovered by the virtual inverse simulations with artificial noise

4.5 Effects of Initial Guess

Suppose the design domain contains many local minima. In that case, an initial guess which is close to the answer will not correctly expose the sensitivity of the forces recovered by the virtual inverse problem (Ben Turkia et al., 2019). To investigate this, ten runs are performed for each method where the initial guess is randomized but remains on average 90% of the answer. For each virtual inverse simulation, samples drawn from a Gaussian random variable with zero-mean and 4N standard deviation are added to the initial guess, after which the usual procedure is followed. The standard deviation of the uncertainty added to the initial guess is more than 10% of the maximum nodal force in the virtual experiments of 35.5N. In addition, similar virtual inverse simulations are run with a "uniform" initial guess, where the initial guess is the same at every node and corresponds to the test section's vertical stiffness multiplied with the total displacement and divided by the number of nodes in contact. The uniform case is statically equivalent to the true answer but can severely over- or under-estimate local forces at a particular node. The same level of artificial measurement noise used in Section 4.4 was retained for all simulations.

Table 4.3 shows the average vertical force and moments predicted by the virtual inverse simulations over ten runs. Although both guesses for both methods show larger moments than when an ideal initial guess is used, the total vertical force is still predicted within 6N (1.6%) in all cases. Table 4.4 shows that both initial guesses for both methods converged to solutions that have very low RMS error on the displacement and strains on the inside of the test section, regardless of whether a displacement-based or a strain-based method was used. However, when considering the force distributions shown in the histograms of the normalized errors, the variance in the forces predicted locally has become very large. Figure 4.3a shows that an initial guess of 90% of the true forces with a large uncertainty still produces a zero-mean distribution of normalized errors, but the variance is around four times as high. The standard deviation for the displacement-based and strain-based methods with this initial guess is 16.4N and 11.6N, respectively. Figure 4.3b shows that the variance is even worse when a uniform initial guess is used, and a multi-modal distribution with high variance appears. For the latter, the standard deviations of the normalized errors for the displacement-based and strain-based methods are 16.8N and 13.3N, respectively.

Table 4.3: Forces and moments predicted by virtual inverse simulations with different initial guesses

Initial Guess	Method	F_z [N]	M_x [Nm]	M_y [Nm]
Reference		359.08	0	0
90% + $\mathcal{N}(0,4)$	Displacement	358.6 ±4	-0.933 ±1.3	0.03853 ±0.4
90% + $\mathcal{N}(0,4)$	Strain	356.6 ±5	-1.239 ±2	-0.1884 ±1
Uniform + $\mathcal{N}(0,4)$	Displacement	364.0 ±2	-1.694 ±2	-0.6371 ±0.2
Uniform + $\mathcal{N}(0,4)$	Strain	357.1 ±2	-1.659 ±0.5	0.07057 ±0.4

Table 4.4: Average root mean square error for the virtual inverse simulations with different initial guesses

Initial Guess	Method	U_x mm	U_y mm	U_z mm	ϵ_{xx} μ	ϵ_{yy} μ	ϵ_{xy} μ
90% + $\mathcal{N}(0,4)$	Displacement	0.03227	0.08697	0.1997	284.4	351.9	226.2
90% + $\mathcal{N}(0,4)$	Strain	0.05158	0.4087	0.4987	911	1029	487.2
Uniform + $\mathcal{N}(0,4)$	Displacement	0.1041	0.6276	0.8744	1569	1895	1082
Uniform + $\mathcal{N}(0,4)$	Strain	0.0446	0.4657	0.4825	930	1027	401.8

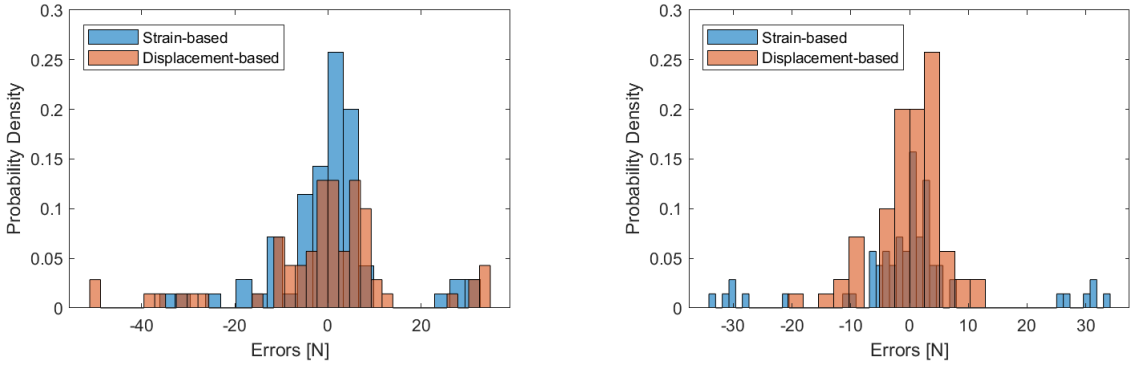

(a) 90% + $\mathcal{N}(0,4)$ (b) Uniform guess + $\mathcal{N}(0,4)$

Figure 4.3: Spread of the local normalized errors on the forces recovered by the virtual inverse simulations with artifical noise and a poor initial guess

4.6 Discussion

From Section 4.4, it is clear that measurement noise does not significantly impact the identifiability of the total vertical contact force in this test case. For a noise level representative of the uncertainty in the deformation measurements, one can expect that the standard deviation of the uncertainty in the force distribution is less than 6% of the total force predicted for the test case. Comparable levels of uncertainty in the strain measurements produce slightly higher but similar levels of uncertainty in the force distribution at 9%. In all cases, the total force predicted by the virtual inverse problem matches the virtual experiment. The standard deviation of the normalized local errors on the forces identified is within 10% of the maximum local force. For this case, it is possible to recover the force distribution over the contact patch.

Section 4.5 shows, however, that the identifiability of the individual contact forces diminishes significantly in the presence of a poor or non-physical initial guess. Despite this, the total force is still acceptably predicted by the virtual inverse problem, even when the distribution of those forces is far from the known solution from the virtual experiment. It is difficult to identify the true solution under non-ideal circumstances, especially if one does not have a good initial guess. Saint Venant's principle dictates that in this case, it becomes increasingly difficult to distinguish between different statically equivalent loads the further away the strains and displacements are observed (Gere and Goodno, 2009). It should be noted that the model has only one element through the thickness of the tyre, so the variation of strain through the thickness of the element is limited by the element type.

The identifiability of the contact forces from deformation measurements is dominated more by the initial guess rather than the measurement noise. In Section 4.4, the initial guess is chosen with the correct shape but a lower magnitude than the true solution, while in Section 4.5, the initial guess can have a non-physical shape. However, the magnitude is still on average lower than the true solution. There is clearly some evidence that if one intends to recover the distribution of contact forces, then the initial guess must be regularized in some way to avoid converging to one of the many local minima that result in non-physical solutions in the solution space. There are many possible methods for regularizing the problem, however in this case it is desirable to ensure that any regularization strategy used does not contain implicit bias from *a priori* knowledge. A regularization strategy biased by expert knowledge or behaviour observed from a simple model is likely to limit the performance of the model when it is expected to include the effects of friction or forces applied in different directions.

4.7 Chapter Summary

This chapter follows the development of an optimisation-based virtual inverse simulation to predict external tyre forces from deformation or strain measurements, where the external forces on the reduced geometry tyre model are altered until the strains or deformations on the inside of the simulation match an expectation from a virtual experiment. The study is conducted for an ideal case with a good initial guess and perfect measurements, followed by one where measurement noise is introduced and finally one where the initial guess is not representative of the true answer. It is found that in the ideal case both the total forces and the individual nodal forces are readily identified. The presence of measurement noise creates a distribution of identified forces, but this distribution is small relative to the total force and the total identified force remains accurate. If the initial guess used is non-physical or its shape is not similar to the true answer, then the optimisation is likely to converge to a solution where the shape of the force distribution is poor. In these cases the total force is still well approximated. It is argued that this is a consequence of Saint Venant's principle, since all the solutions are statically equivalent but difficult to distinguish as the measurements are not in the same location as the load application. This chapter demonstrates that the problem requires regularization.

Chapter 5

Regularization Investigation

5.1 Overview

In Chapter 4 an optimisation-based approach was used to estimate the degree to which external forces can be inferred from deformations and strains. This approach has the unfortunate consequence that many simulations are run of which only the data from the final simulation is considered to be a valid solution. If we constrain the input space such that only realistic tyre loadings are simulated, then one can infer sensitivities and trends directly from the data. In this section a data-driven strategy is investigated for its suitability to better understand the identifiability of tyre forces from deformation measurements. A dataset for this study is generated using the full geometry model, fixed at 200kPa, for a range of displacements from 10mm to 40mm in increments of 5mm. For this study the pressure was fixed at 200kPa to generate large external forces distributions. The dataset generated for this study has a single latent variable which is the total deformation on the tyre. This is in contrast to Chapter 4 where the design space is not limited (the forces at all 14 nodes in contact were used to describe the force distribution). In this chapter the raw dataset is regularized by the latent variable to only include strains, deformations, and forces from the quasi-static loading of an inflated slick tyre against a frictionless, flat road. The first study uses Principal Component Analysis to determine if it is possible to reduce the dimensionality of the problem, and to better understand how the virtual measurements inform one about the external forces. The second study models the relationship between the internal deformations and strains and the outer forces using Principal Component Regression and Partial-Least Squares Regression. Partial-

Least Squares Regression is then used to repeat the sensitivity studies performed in Section 4. The result of this investigation allows one to reduce the input space to only those regions of the inner tyre which are highly informative about the external forces.

5.2 Typical Regularization Strategies

Regularization methods typically introduce some bias into the problem to be solved in order to prevent over-fitting, and usually involve modifying the cost function, the data sampling, or the training approach if parameters are to be fitted (Svensén and Bishop, 2007). In the context of the virtual inverse problem one can therefore alter the cost function and/or the data sampling to achieve regularization.

Common methods for regularizing the cost function typically exist to drive sparsity or smoothness. Sparsity can be encouraged by adding an L1 or L2 penalty to the cost function, where the sum of the input vector or the square of the sum of the input vector respectively is added to the error. On the other hand, smoothness can be achieved by penalizing deviations of the error function by a pre-determined shape such as a parabola. In the case of L1 and L2 regularization the physical consequence is similar to only searching for solutions where the external forces are as close to zero as possible. Such a regularization strategy might guarantee that forces which should be zero are appropriately identified, but will always bias the solution towards low forces spread over a large area. Smoothness can be encouraged by penalizing deviations of the deformations or strains from a pre-determined function, such as a parabola or some arbitrary phenomenological function. There has been considerable research regarding the shape of the strain components on the inside of a tyre for different loading scenarios (Holtschulze et al., 2005; Matsuzaki et al., 2010; Lee and Taheri, 2019; Garcia-Pozuelo et al., 2019a), which reveals that the strain components do in fact have a predictable shape in some scenarios. These strain profiles will change drastically in scenarios where the tyre moves over rough roads, obstacles, deformable terrains and if the tyre is subject to lateral, longitudinal or combined loadings. Therefore, regularization involving a smoothing strategy is likely to limit the space of possible solutions to those observed before.

The data itself can also be used to regularize the problem. This typically takes the form of data augmentation or k-fold cross-validation. Data augmentation involves randomly cropping,

scaling, rotating, and injecting noise into the data, while in k-fold cross-validation the data is divided into k groups, the model is trained on (k-1) groups and tested against the remaining data for all k combinations. These strategies may not apply directly to the model explored in Section 4 as it is not trained like most models in data science, however one can still explore the possibility of using the data from the virtual experiments more selectively as it is likely that some data are more informative than others. This idea is explored in Section 5.3. Similarly, the virtual deformation measurements can be used to formulate a physically-meaningful regularization strategy. Since the tyre's material properties are nearly incompressible the thickness of the tyre is likely to remain nearly constant during loading. If one offsets the geometry of the deformed inner surface of the tyre by the thickness, then this can be applied as a deformation boundary condition in FEM to recover external reaction forces and thus an initial guess.

5.3 Principal Component Analysis

One challenge faced by the optimisation algorithm is that the input space is large, and many terms have little influence over the objective function. Similarly, the virtually measured deformations/strains which are used to penalize deviations from the true answer are also high-dimensional of which few are likely to have a strong relationship with the external force. If one generates a virtual experiment data-set of many possible tyre loading conditions then one can leverage Principal Component Analysis (PCA) to reveal, for the given dataset, where the strongest correlation between the input and output variables lies. This allows one to find which specific regions of the inside of the tyre explain most of the variance in the external force, as well as how much of the variance those regions explain. This can be done by analysing the principal components of the cross-correlation between the nodal deformation/strain and external forces for the given data-set. Once all the simulations in the data set are run, the inputs and outputs are defined as

$$\boldsymbol{X}_{\epsilon} = \begin{bmatrix} \epsilon_{11} & \epsilon_{12} & \dots \\ \vdots & \ddots & \\ \epsilon_{K1} & & \epsilon_{KN} \end{bmatrix}$$

$$\boldsymbol{X}_U = \begin{bmatrix} U_{11} & U_{12} & \dots \\ \vdots & \ddots & \\ U_{K1} & & a_{KN} \end{bmatrix}$$

$$\boldsymbol{Y} = \begin{bmatrix} F_{11} & F_{12} & \dots \\ \vdots & \ddots & \\ F_{K1} & & F_{KM} \end{bmatrix}$$

where K virtual experiments are considered, with N nodes on the inside of the tyre and M nodes on the outside of the tyre. The input matrices $\boldsymbol{X}_\epsilon$ and $\boldsymbol{X}_U$ contain all the N nodal strains and displacements (for a particular direction) over all K virtual experiments, while the output matrix $\boldsymbol{Y}$ contains all the M nodal reaction forces over the same K virtual experiments. Therefore over the dataset there are 6 input matrices (one for each direction of strain and deformation), and one output matrix. The strain referred to here simply as ϵ is the strain extrapolated from the integration points to nodal locations as explained in Section 4.2. One can calculate the cross-covariance $\boldsymbol{T}$ between any mean-centered input matrix ($\bar{\boldsymbol{X}}_{\boldsymbol{\epsilon}}$, $\bar{\boldsymbol{X}}_{\boldsymbol{U}}$) and the mean-centered output matrix ($\bar{\boldsymbol{Y}}$) as

$$\boldsymbol{T} = \bar{\boldsymbol{X}}^{\boldsymbol{T}}\bar{\boldsymbol{Y}} \tag{5.1}$$

where $\bar{\boldsymbol{X}}$ is any $\bar{\boldsymbol{X}}_{\boldsymbol{\epsilon}}$ or $\bar{\boldsymbol{X}}_{\boldsymbol{U}}$ for a particular direction. The cross-covariance matrix $\boldsymbol{T}$ is generally non-square and therefore one cannot extract the principal components using a normal eigenvalue decomposition. Instead one can use the Singular Value Decomposition (SVD) of the cross-covariance to extract the same information, which is defined as

$$\boldsymbol{T} = \boldsymbol{W}\boldsymbol{\Sigma}\boldsymbol{V}^T \tag{5.2}$$

where $\boldsymbol{W}, \boldsymbol{V}$ are real, orthogonal matrices and $\boldsymbol{\Sigma}$ is a non-square matrix whose only non-zeros entries lie on the main diagonal. The product $\boldsymbol{W}\boldsymbol{\Sigma}\boldsymbol{V}^T$ reconstructs the original cross-covariance matrix $\boldsymbol{T}$. In this case the $\boldsymbol{W}$ matrix can be viewed as the "eigen-displacement" or "eigen-strain" matrix, and similarly the $\boldsymbol{V}$ matrix can be interpreted as the "eigen-forces" matrix. The $\boldsymbol{\Sigma}$ matrix is analogous to the eigenvalues in the eigenvalue decomposition of a square matrix, but it has as many diagonal entries as the smallest dimension of the problem. The $\boldsymbol{\Sigma}$ matrix contains the singular values/principal components of $\boldsymbol{T}$. One can re-construct the original matrix $\boldsymbol{T}$ with one or more of the principal components by selecting those components in $\boldsymbol{\Sigma}$

which are desired, setting the rest to zero, and performing the product $\boldsymbol{W}\boldsymbol{\Sigma}\boldsymbol{V}^T$. The entries in $\boldsymbol{\Sigma}$ are arranged in descending order of magnitude, and the larger the magnitude of an entry in $\boldsymbol{\Sigma}$ the higher the influence that particular combination of displacements and strains has on the forces. Therefore, plots of just the principal components of the cross-correlation indicates the dominance of each "mode" of $\boldsymbol{T}$. Based on the principal components one can get a clear understanding of which regions of the tyre explain the most variance of the external forces. The columns and rows of $\boldsymbol{W}, \boldsymbol{V}^T$ are hierarchically ordered such that the columns of $\boldsymbol{W}$ and the rows of $\boldsymbol{V}^T$ each explains the variance of $\boldsymbol{T}$ from highest to lowest. As such, the entries in the first column and row of $\boldsymbol{W}$ and $\boldsymbol{V}^T$ respectively explains the most variance.

5.3.1 Influence of Deformation Measurements

Figure 5.1 shows the principal components of the cross-covariance between the interior deformation measurements and exterior forces for the dataset. The top plot shows all of the principal components in a logarithmic scale, while the bottom plot shows the first three principal components in a linear scale. One would expect that U_z measurements explain most of the variance in the external forces, and this is confirmed by Figure 5.1. It is also clear that the vast majority of the variance in the external forces can be attributed to the first principal component of the measurements, which matches the hypothesis that the problem has essentially a single degree-of-freedom problem since it involves only vertical displacements on a frictionless plate. The principal components tend to have similar values for many nodes which is explained by the fact that adjacent nodes are likely to have similar displacements, and therefore a similar principal component. If one isolates the first column of the $\boldsymbol{W}$ matrix (the "eigen-deformation" matrix) from the SVD then a heat-map can be generated which can be used to show to what degree each measurement on the inside of the tyre contributes to explaining the variance in the external force, which is pictured in Figure 5.2 for each direction. In the three right-hand plots of Figure 5.2 the contributions are normalized according to their highest principal component compared to the highest principal component for all directions (U_z in this case), which makes it clear which directions are more important than others. In the three left-hand plots the figures are not normalized. One can see that measurements on the inside of the tyre in the region of the contact patch explain most of the variance, less is explained by the sidewall adjacent to the contact patch, and almost none is explained by the rest of the measurements. If one has all three components of deformation available then it is sensible to only measure U_z near the contact patch, but it would also be feasible to measure U_y at the sidewall near to the contact patch. The bottom right-hand plot shows that there is still a relationship between the U_x deformations and the external force, despite the fact that these measurements explain little of the variance in the external forces.

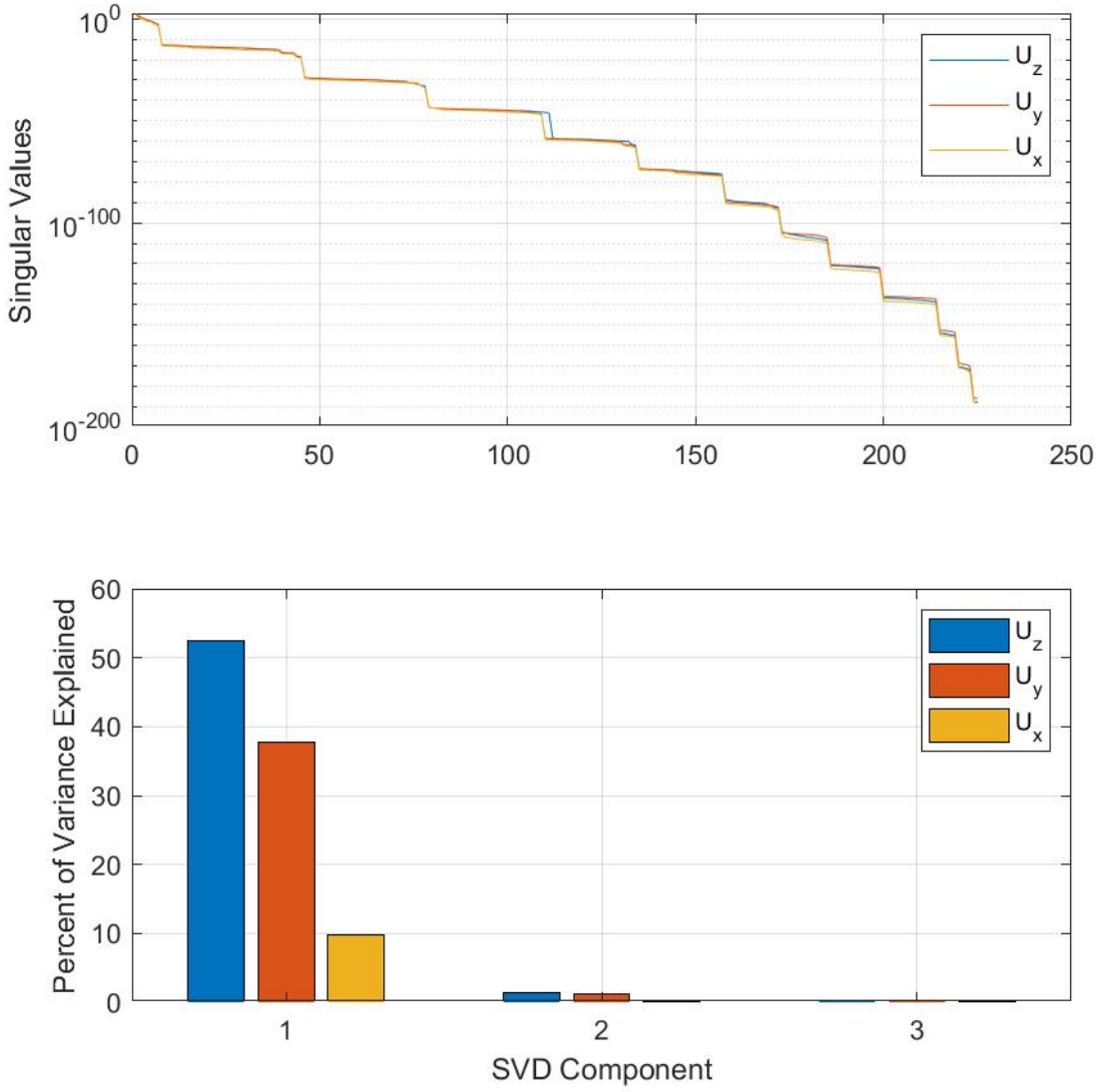

Figure 5.1: Principal Components of the cross-covariance between internal displacements and external forces

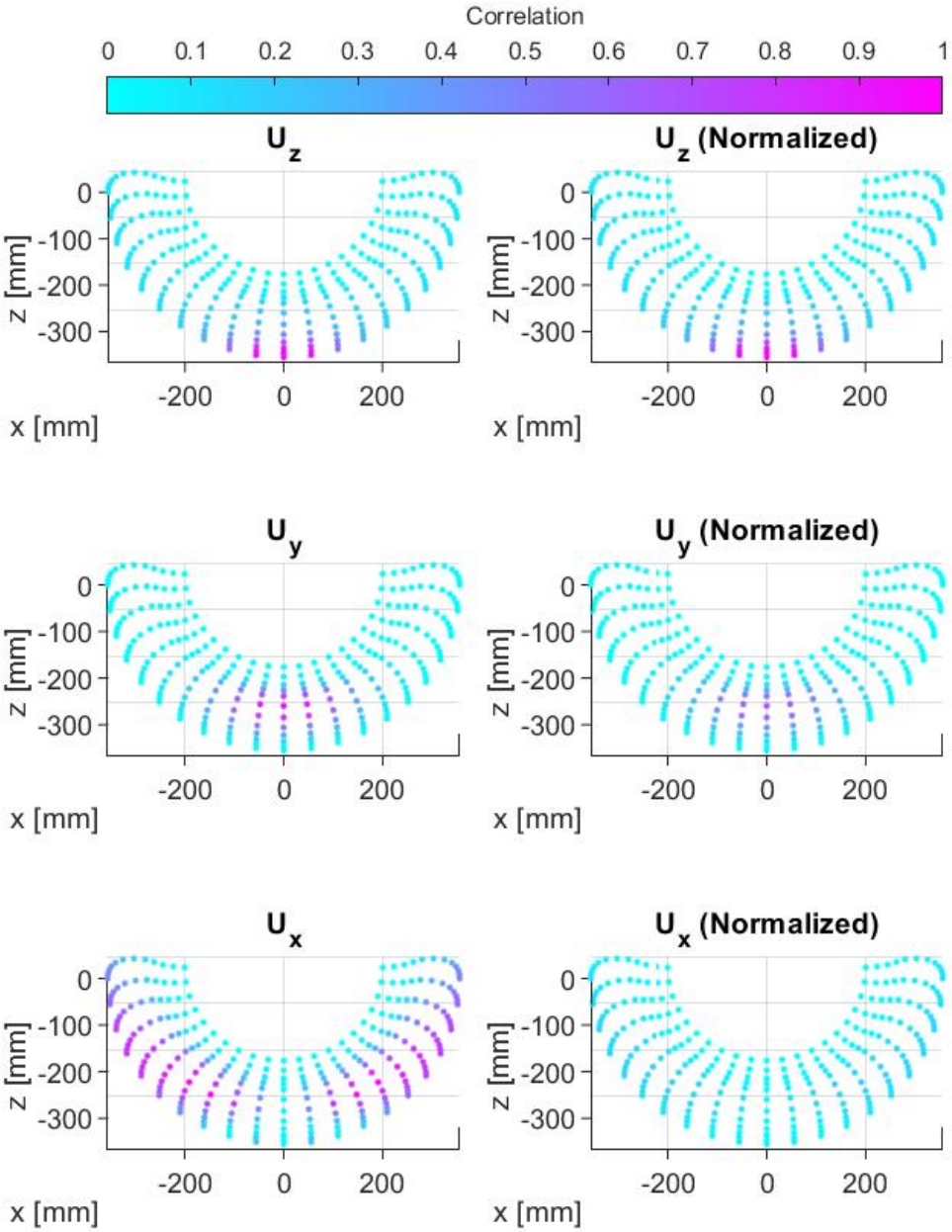

Figure 5.2: Normalized and un-normalized plots of the correlation between internal deformations and external forces

5.3.2 Influence of Strain Measurements

Repeating the same procedure described in Section 5.3.1 except with internal nodal strains instead of deformations results in Figures 5.3 and 5.4. As before the majority of the variance in the external forces is explained by the first principal components of all the strains. Figure 5.3 shows that ϵ_{xx} explains most of the variance in the external force, followed by ϵ_{yy} and finally ϵ_{xy} although in this case ϵ_{xy} is a third as informative as ϵ_{xx} whereas in Section 5.3.1 U_x was around one-fifth as informative as U_z. One can say that each component of strain is individually less informative but the spread between them is lower. This agrees with the work in projects APOLLO and FRICTI@N (The European Commission, 2005, 2008) which claims that optical measurements, and thus deformations, are the preferred measurement type for an intelligent tyre. The heatmap of the "eigen-strains" is shown in Figure 5.4 where there are normalized and un-normalized plots for each direction as in Section 5.3.1. It is clear form Figure 5.4 that although ϵ_{xx} and ϵ_{yy} are most informative about external forces, the region of nodes with a significant correlation is spread out over a larger area than in Figure 5.2. The left-hand three plots in Figure 5.4 show that the nodes which are informative about the external forces all lie in a region much larger than the contact patch. Additionally each component of strain is informative in similar regions which is in contrast to Figure 5.2 where each direction of deformation is informative in a different region. All three strain components are highly informative in the region of the tyre where the sidewall meets the tread, and similar results were found by Feldesi et al. (2020) where T2Cam was found to measure high strain values in the same location. The fact that strains are less informative overall compared to displacements is convenient for developing a model for an optical-based intelligent tyre like T2Cam, since calculating the strain requires taking a derivative which is known to induce numerical inaccuracies from noise.

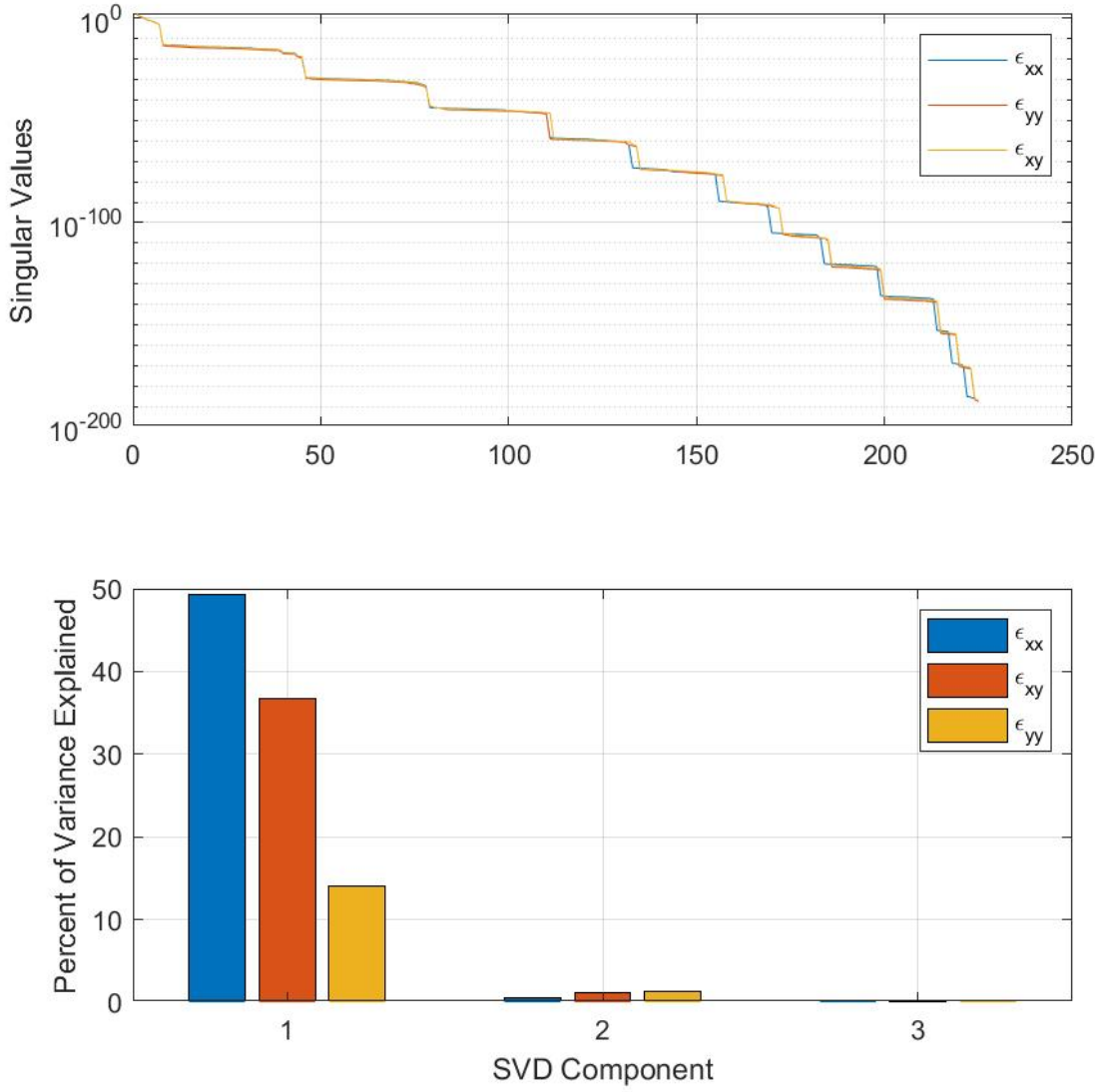

Figure 5.3: Principal Components of the cross-covariance between internal nodal strains and external forces

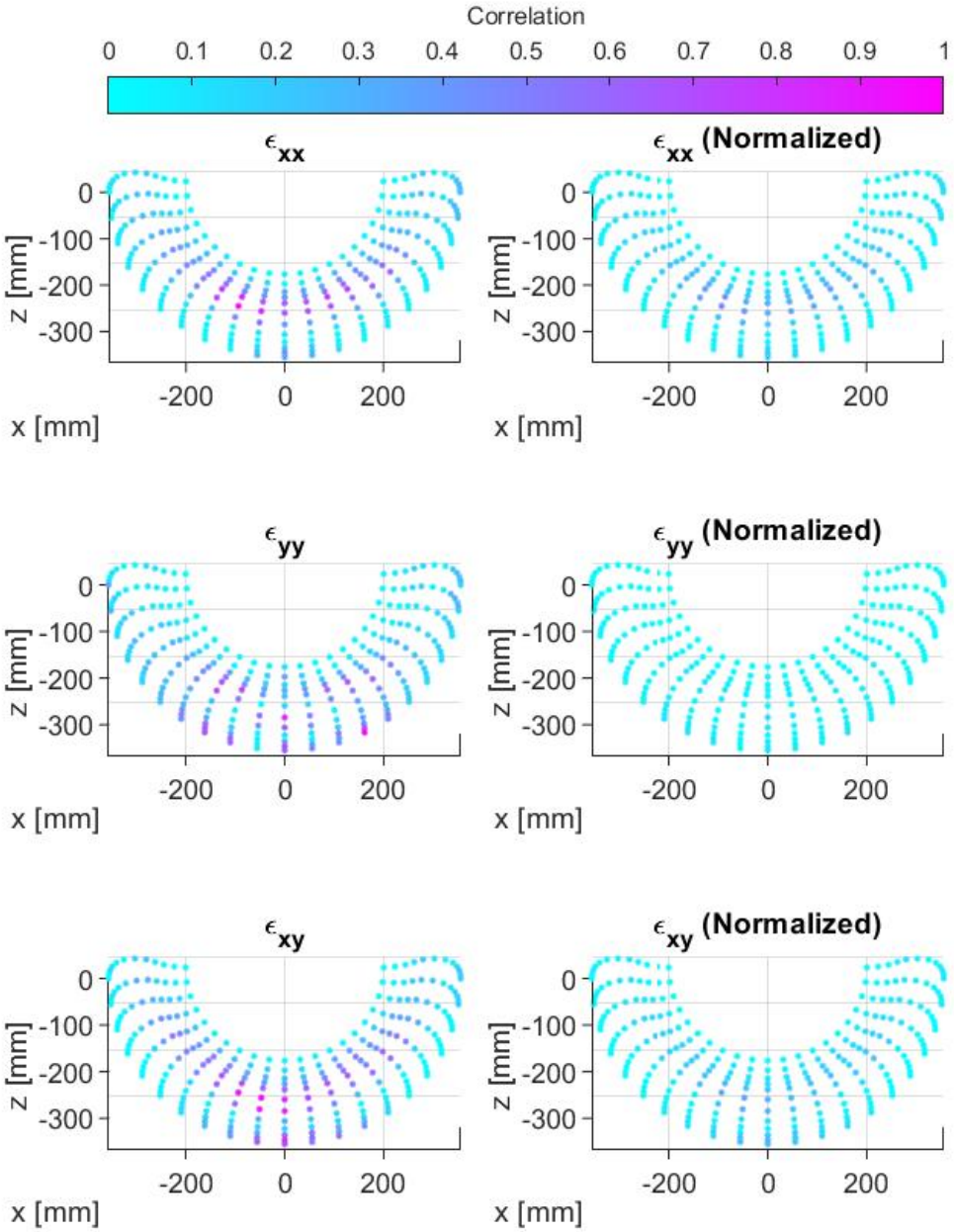

Figure 5.4: Normalized and un-normalized plots of the correlation between internal nodal strains and external forces

5.4 Principal Component Regression

In Section 5.3 it was shown that there exists an identifiable latent variable between the deformations and strains on the inside of the tyre which explains the majority of the variance in the external forces. In this section a supervised Principal Component Regression (PCR) is performed to reconstruct the "eigen-forces" from the "eigen-strains" and "eigen-deformations", where one can choose how many modes to use in the reconstruction. Principal Component Regression is a linear orthogonal map of the input space to the output space, where the directions used for the mapping are derived from the principal components of the input and output vector.

Consider the zero-mean input matrices $\bar{\boldsymbol{X}}_{\boldsymbol{\epsilon}}$ and $\bar{\boldsymbol{X}}_{\boldsymbol{U}}$ described in Section 5.3 and the corresponding zero-mean output matrix $\bar{\boldsymbol{Y}}$. The input matrices are of a different shape to the output matrix since there are a different number of nodes on the inside of the tyre compared to those on the outside. One can construct a linear model on the eigenvectors of the input and output matrices, which will map the direction of maximum variance in the input to the direction of maximum variance in the output. First, the covariance matrix for the input $\boldsymbol{K}_{\boldsymbol{X}}$ and output $\boldsymbol{K}_{\boldsymbol{Y}}$ are calculated as

$$\boldsymbol{K}_{\boldsymbol{X}} = \boldsymbol{X}^T\boldsymbol{X}, \text{ and} \tag{5.3}$$

$$\boldsymbol{K}_{\boldsymbol{Y}} = \boldsymbol{Y}^T\boldsymbol{Y} \tag{5.4}$$

The eigenvectors $\boldsymbol{u}$ and eigenvalues λ of each covariance matrix are calculated. One chooses r^* columns of the input and output eigenvector matrix, and calculates the scores $\boldsymbol{Z}$ for both matrices

$$\boldsymbol{Z}_{\boldsymbol{X}} = \boldsymbol{X}\boldsymbol{u}_{\boldsymbol{X}}{}^*, \text{ and} \tag{5.5}$$

$$\boldsymbol{Z}_{\boldsymbol{Y}} = \boldsymbol{Y}\boldsymbol{u}_{\boldsymbol{Y}}{}^* \tag{5.6}$$

A linear model with weights α is then constructed on the input and output scores $\boldsymbol{Z}_{\boldsymbol{X}}$ and $\boldsymbol{Z}_{\boldsymbol{Y}}$

$$\boldsymbol{Z}_{\boldsymbol{Y}} = \alpha\boldsymbol{Z}_{\boldsymbol{X}}. \tag{5.7}$$

Given a particular input one can reconstruct the output by multiplying the input vector by $\boldsymbol{u}_X^*$, then taking the product $\alpha \boldsymbol{Z_X}$, and finally solving $\boldsymbol{Z_Y} = \boldsymbol{Y}\boldsymbol{u}_Y^*$. Therefore PCR models the response of a variable by linearly mapping the directions of maximum variance in the input and output space. It should be noted that PCR will be successful if one intends to map the directions of maximum variance of the input space to the output space, which may not represent the actual relationship between these quantities depending on how the data was generated. One can approximate a non-linear relationship between the input and output space by choosing to model it with as many modes as required to achieve the desired accuracy, even though the model itself is still linear in the principal component space.

Figures 5.5 and 5.6 shows the tread forces predicted by the PCR model from displacement and strain respectively for varying numbers of modes for a total displacement of 30mm at 200kPa inflation pressure. The predictions using 3 or more principal components shows good correlation with the reference virtual experiment results. The eigenvalues of the output covariance matrix can be used to plot the percent of variance explained in the output by each mode, which is shown in Figure 5.7. The first and second modes only explain 64% and 78% of the variance in the output respectively, while the third mode increases this to 91%. The dataset comprises of virtual experiments wherein there is a single known latent variable which is the total displacement of the tyre. The non-linearity of the tyre means that it is not accurate to model this relationship using a linear mapping with a single variable, and as such a PCR model with one mode is not sufficient to represent the relationship between displacements or strains on the inner surface of the tyre and the distribution of forces on the outside. This shows that although it is relatively easy to identify the latent variable, modelling it in a low dimensional space may be difficult. However it is clear that using three or more modes are sufficient to model the non-linear behavior of the tyre with linear variables. While it is clear that PCR is able to construct maps between the internal deformations/strains and the external forces, there is no guarantee that the direction of maximum variance in the output corresponds to that of the output. A more robust approach is presented in Section 5.5 whereby the input direction is varied to maximise the variance in the output explained by the input using Partial-Least Squares Regression (PLSR).

5.5 Partial Least Squares Regression

PCR is an attempt to use unsupervised methods to model a supervised problem. This has the consequence that if the directions of maximum variance in the input space do not map well

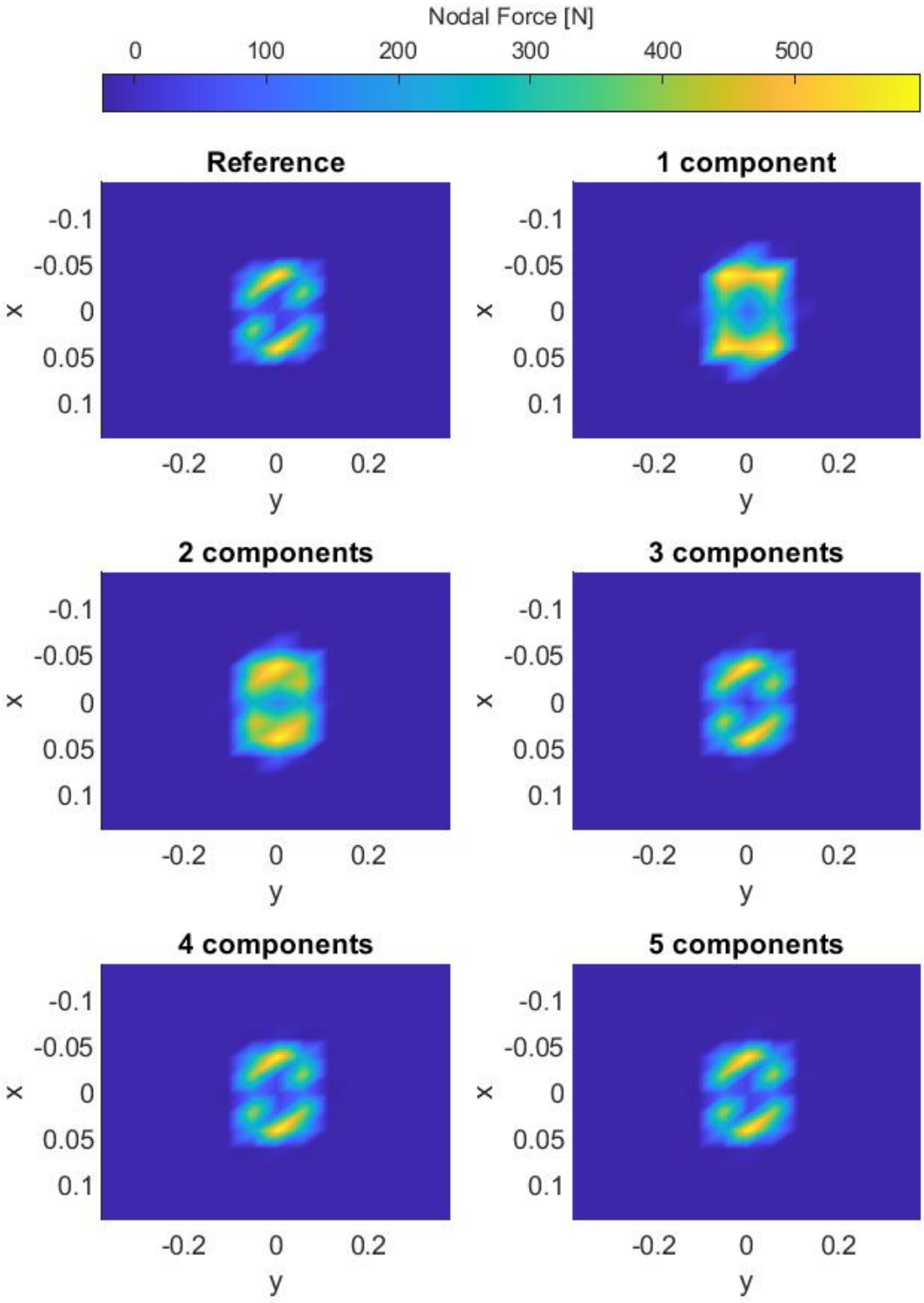

Figure 5.5: Tread forces predicted from displacements with a PCR model for varying number of modes

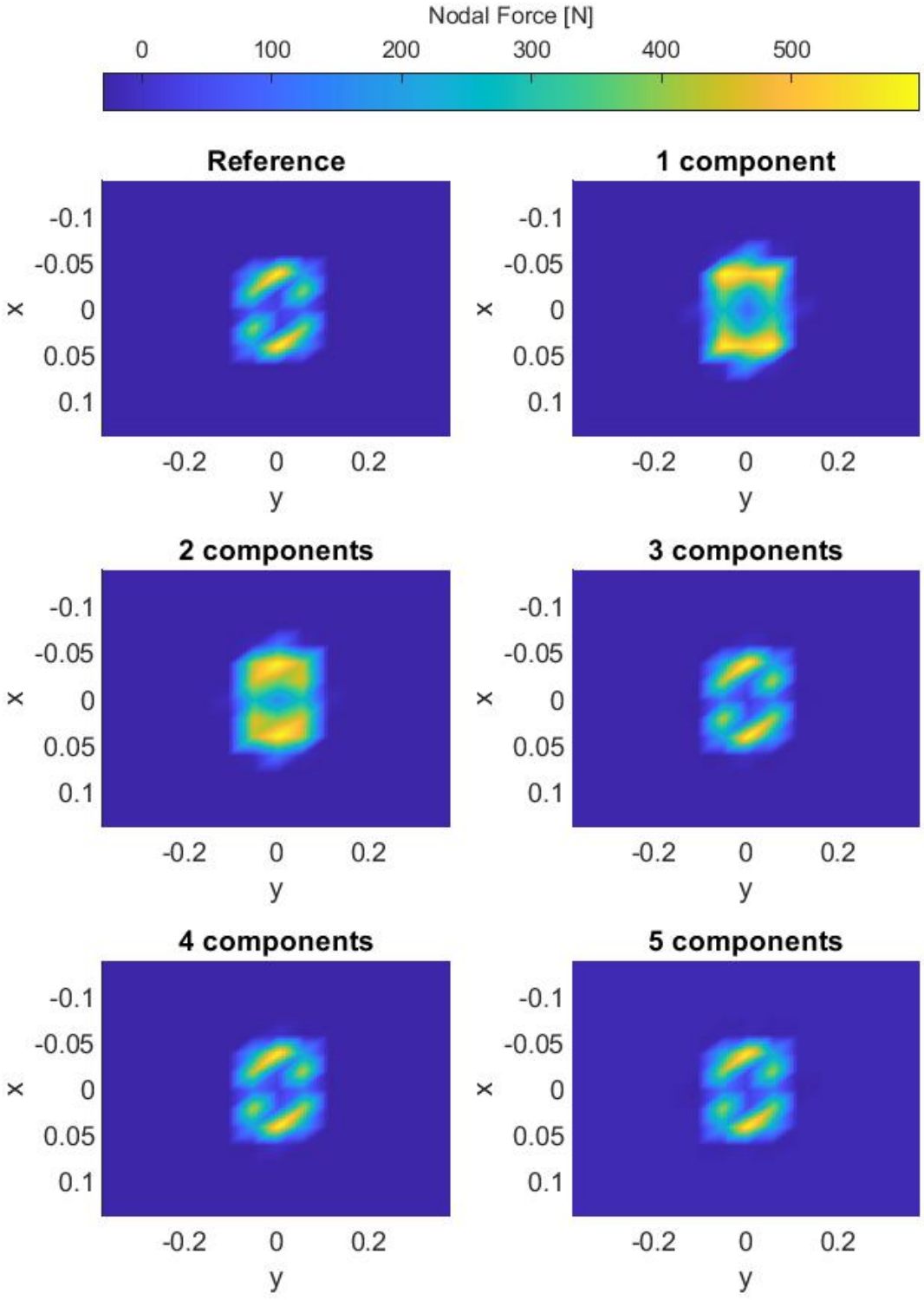

Figure 5.6: Tread forces predicted from strains with a PCR model for varying number of modes

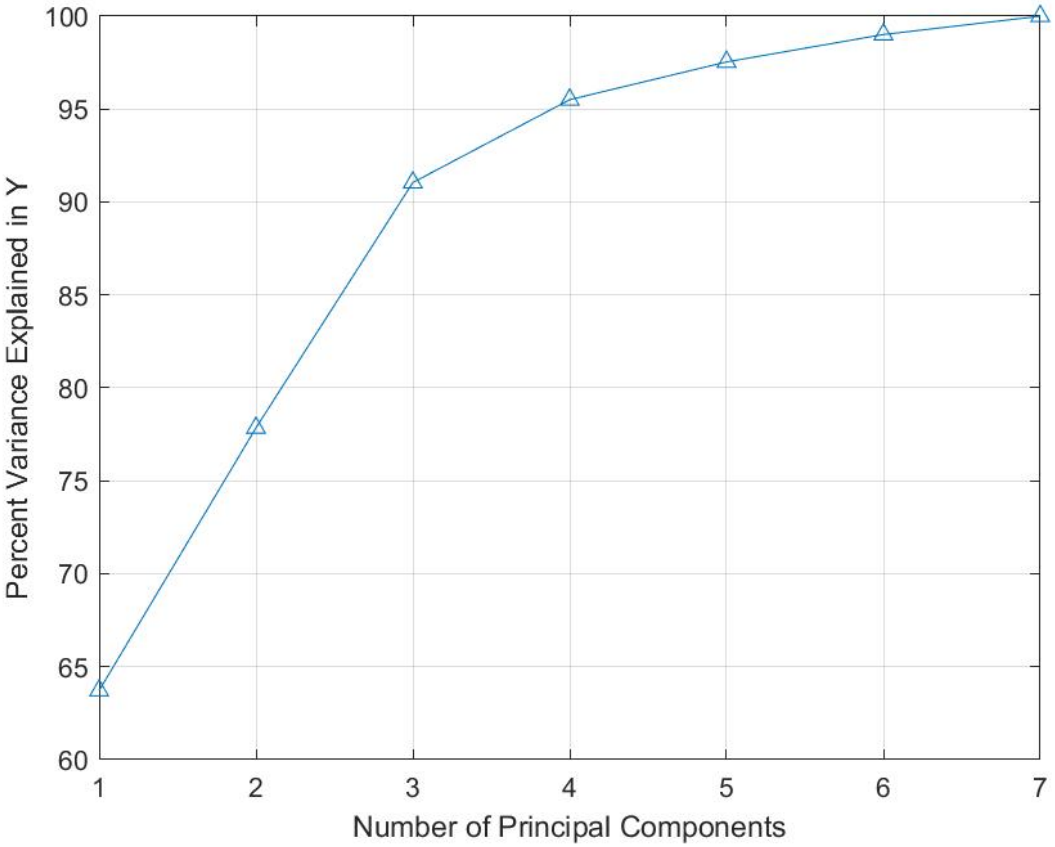

Figure 5.7: Percent of variance in the output explained by each mode of the PCR

to those of the output space then the reconstructions will always be poor. Instead of simply mapping the directions of maximum variance in the input to the output, we can instead look for a direction which has a high correlation between the input and output. Partial Least Squares (PLS) regression is one method for doing this. PLS attempts to maximise the covariance between the inputs and output reconstruction by iteratively choosing different directions to map between. PLS is structurally the same as PLR as it has scores and loadings, but it is not fixed to one set of loadings as it can vary the directions. There are many algorithms available for performing PLS regression and in this case the algorithm SIMPLS developed by De Jong (1993) as implemented in MATLAB will be used. Similarly to PCR, PLS is a linear orthogonal map of the input space to the output space, but only the direction for the mapping of the output is derived from principal components.

As in Section 5.4 the tread forces for a 30mm total displacement virtual experiment at 200kPa inflation pressure are shown in Figures 5.8 and 5.9 for the displacement-based and strain-based methods respectively. The predictions made by the PLS model behave similarly to PCR whereby

the tread forces are nearly perfect if 3 or more modes are used. Both methods are related by their use of principal components, so this behavior is expected. Figure 5.10 shows the percent of variance explained in Y for the displacement-based and strain-based PLS regression methods as well as that of PCR. Since the PLS regression varies the input direction to maximise variance in the output, the percent of variance explained in the output is slightly different for the two PLS regression methods. It is clear that PLS regression is more efficient at explaining the variance in the output when more than 1 mode is used. The displacement-based method explains 53.8%, 79.5% and 95.2% for the first three modes respectively, while the strain-based method explains 52.9%, 79.6% and 96.9% for the same modes. If one uses the PLS regression model with 3 or more modes then it is possible to get fast and accurate function evaluations of the external forces from the internal displacement or strain, without having to run the virtual inverse simulation from Section 4. This method does not suffer from the effects of an initial guess but is not reliable for identifying loading scenarios outside of the dataset that was used to train the PLS model. This tool allows one to revisit the effects of noise studied in Section 4.4 without concerns of optimisation-related effects. This is the topic of Section 5.6.

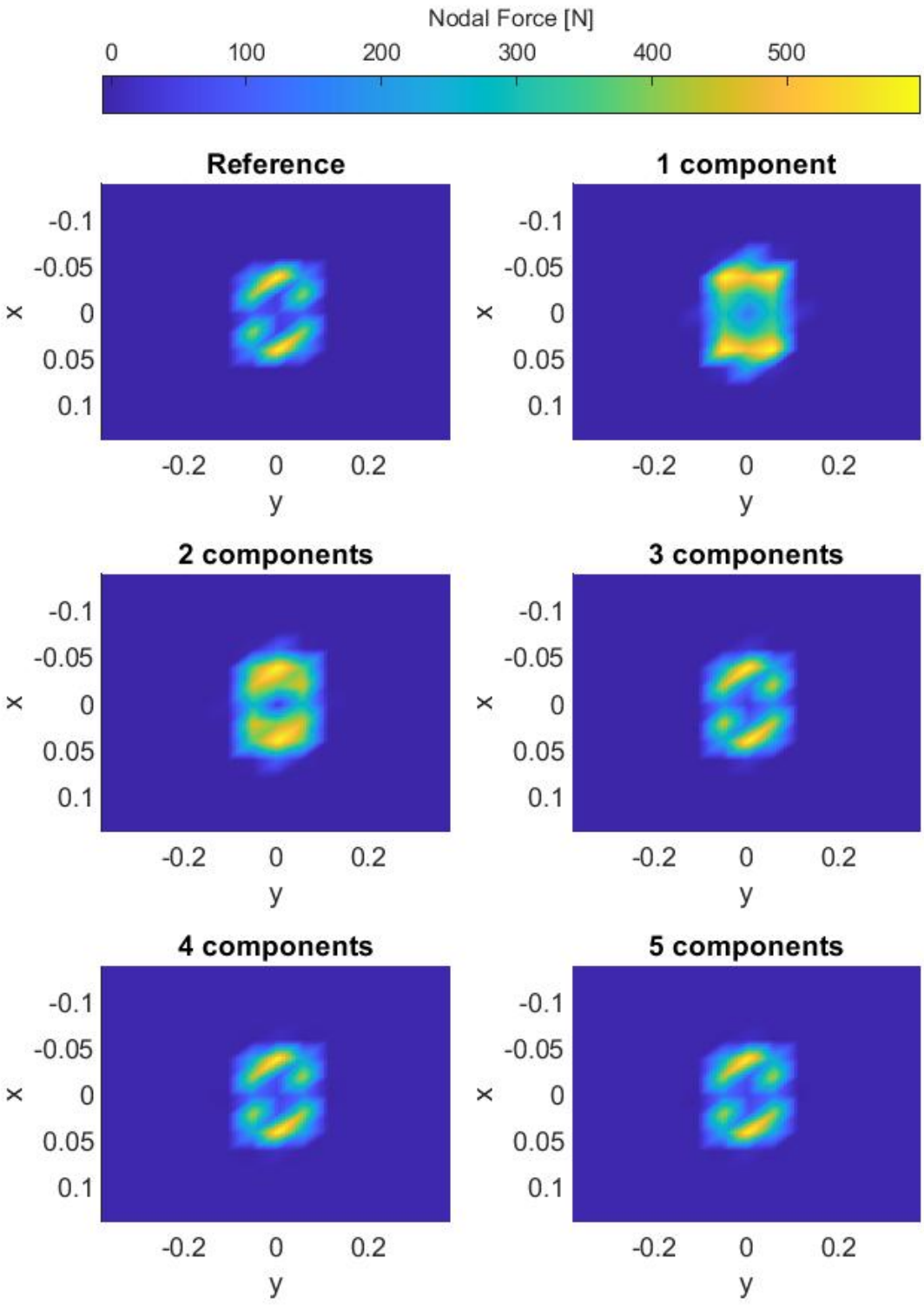

Figure 5.8: Tread forces predicted from displacements with a PLSR model for varying number of modes

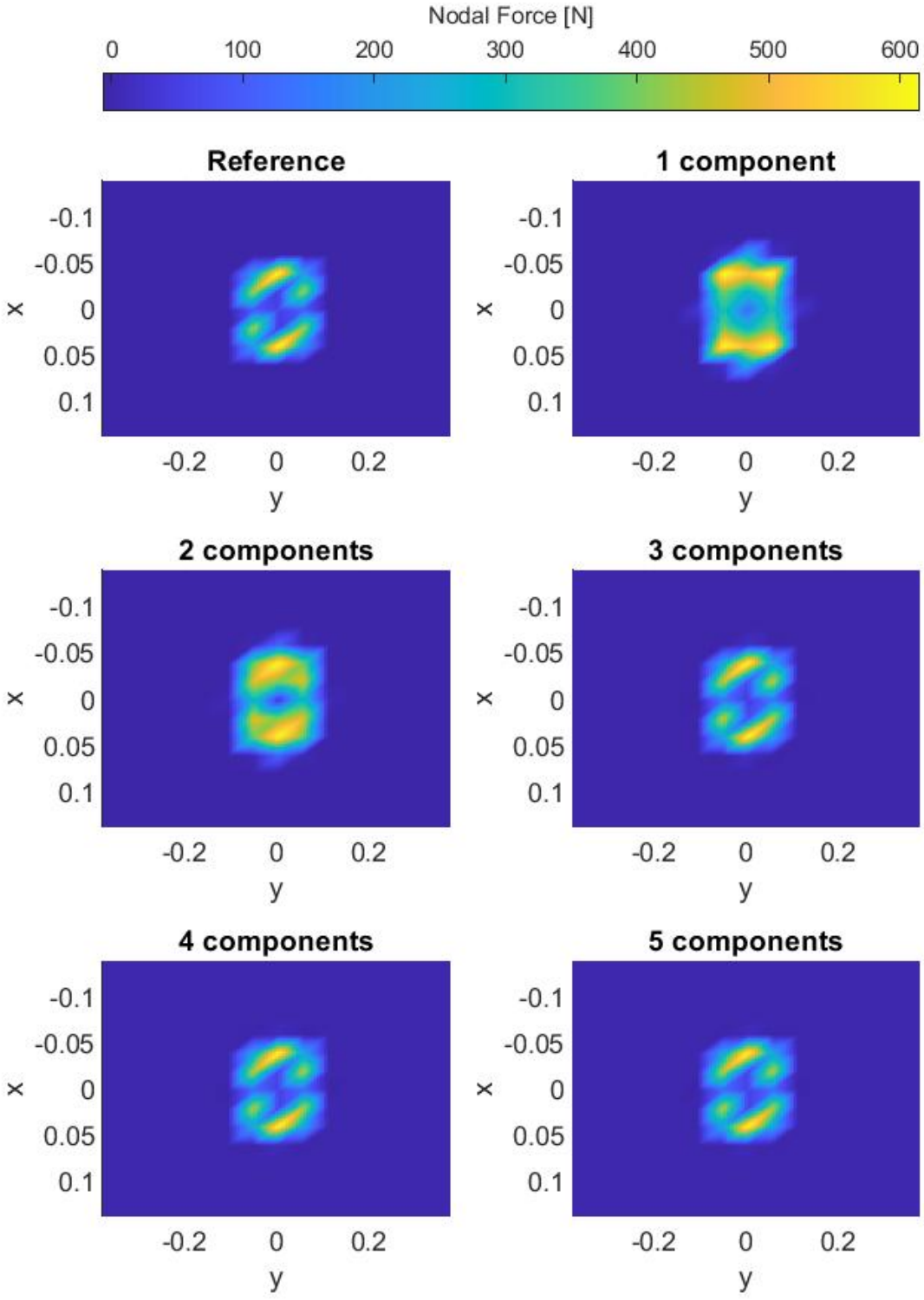

Figure 5.9: Tread forces predicted from strains with a PLSR model for varying number of modes

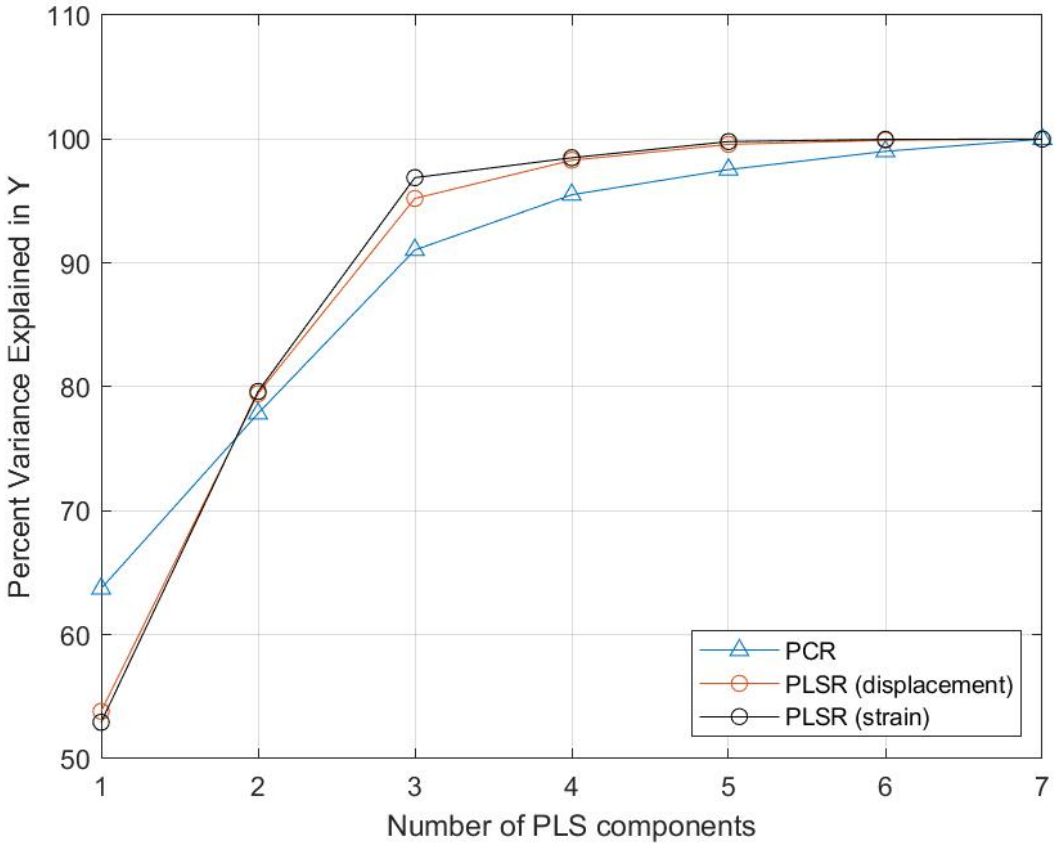

Figure 5.10: Percent of variance in the output explained by each mode of the PLSR compared to PCR

5.6 Parameter Sensitivity with PLS Regression

A virtual inverse simulation was used to investigate whether or not external forces can be identified from internal deformations or strains in Section 4. However it was difficult to separate the effect of optimisation due to vast plateaus in the design space. In this section PLS regression will be used to revisit the identifiability investigation.

The inputs to the method of PLS regression discussed in Section 5.5 are the strains or deformations from the inner surface of the tyre, obtained from a virtual experiment. Similarly to Section 4.4 one can super-impose zero-mean noise on these virtual measurements and then evaluate the PLS model and compare the distribution of predicted external forces to those found in the virtual experiment. This process was repeated 100 times for the same noise level as in Section 4.4 ($\mathcal{N}(0,1)mm$ on displacement and $\mathcal{N}(0,0.04)\%$ on strain) which resulted in a distribution of external forces at each nodal location. This process was carried out at a fixed total displacement and pressure of 30mm and 200kPa respectively to rule out the effect of pressure and total displacement on the results.

Figure 5.11 shows the mean error and standard deviation of the external forces at the contact patch for both the displacement-based and strain-based methods. The mean tread force error shown in Figure 5.11a indicates that on average PLS regression with a noisy measurement will correlate with the corresponding virtual experiment. The maximum error is 60.7N and 32.9N for the displacement-based and strain-based methods respectively, which amounts to 1.4% and 0.7% of the total force or 23.4% and 12.7% of the average nodal force. The standard deviation of the external forces is shown in Figure 5.11b and is mostly concentrated around two regions just infront of and behind the centerline of the tyre. The total force for this virtual experiment is 4.5kN and the maximum standard deviation of the external forces is 600N, meaning that the standard deviation can be up to 13% of the total force. The average nodal external force in the corresponding virtual experiment (excluding nodes that are not in contact with the road) is 259N, and as such the maximum standard deviation is 231% of the average nodal force. These results are tabulated in Table 5.1 for both methods with and without noise. Table 5.1 also includes the nodal averaged standard deviation on the external force distribution. Although the maximum standard deviation of the total forces is high, the nodal averaged standard deviation is only 133.13N and 149.28N for the displacement-based and strain-based methods respectively.

The average total moments in the x and y directions, as well as their nodal-averaged standard deviations, are also reported in Table 5.1. It is difficult to interpret the magnitude of these

moments' standard deviation as the expected moment is zero, but one can instead resolve them to a force applied at the edges of the contact patch as in Section 4.3. The contact patch is approximately 100mm wide in the x-axis and 200mm wide in the y-axis. From the size of the contact patch, the M_x standard deviations are statically equivalent to a force 20x larger while the M_y standard deviations are statically equivalent to a force 10x larger. Therefore the M_x standard deviations are statically equivalent to forces of 257.4N and 177.N applied at the edges of the contact patch for the displacement-based and strain-based methods respectively. Similarly, the M_y standard deviations are equivalent to forces of 155.6N and 115.9N applied at the edges of the contact patch for the displacement-based and strain-based methods respectively. The average nodal standard deviation of the moments are of similar magnitude to that of the average nodal force.

In Section 4 the average total forces and moments identified by the virtual inverse simulation were easily identified but the exact distribution was difficult to identify. The process was time-consuming and as such few virtual inverse simulations were run. With the PLS regression method both training the model and evaluating it are much faster. This allows one to carry out much more statistically significant investigations. To demonstrate this the noise level applied to the inputs of the PLS regression models was varied and evaluated 100 times for each noise level. The results are shown in Figure 5.12 where the nodal average standard deviation (blue) and average total force (orange) is plotted at each noise level for both methods. The average total force remains constant while the nodal average standard deviation increases linearly. Figure 5.12 is useful not only to determine to what extent the distribution of external forces can be identified for a particular scenario, but also to inform the initial design of a particular intelligent tyre; One can determine in what range the measurement noise for certain hardware will lie and therefore the expected distribution of identified external forces.

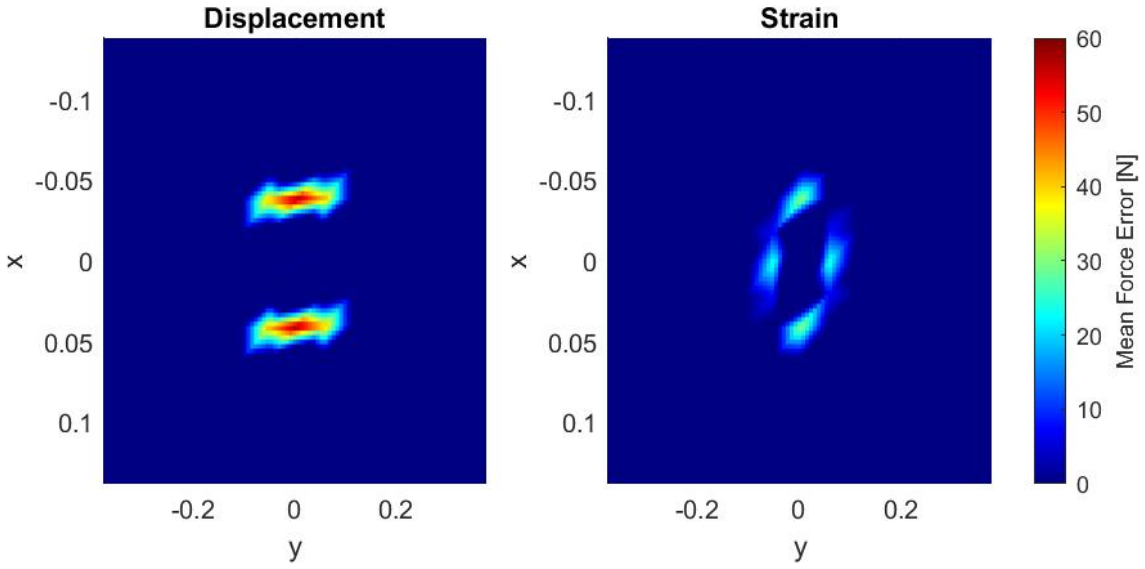

(a) Mean

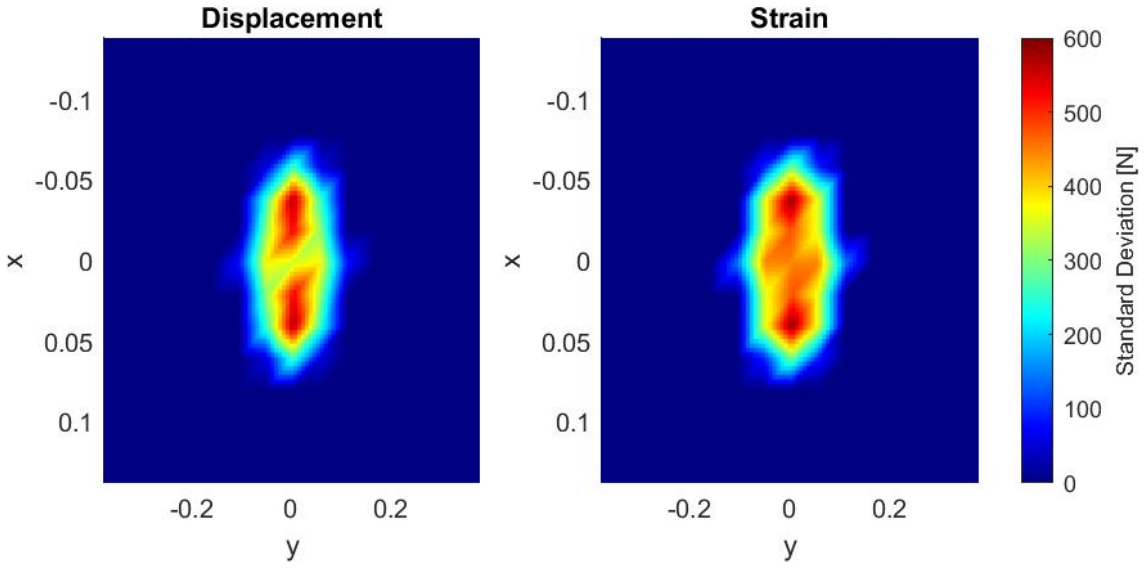

(b) Standard Deviation

Figure 5.11: Mean and standard deviation of the external faces

Table 5.1: Total forces and moments predicted by PLSR with and without noise

	F_z N	M_x Nm	M_y Nm
Reference	4475.70	0	0
Displacement-based	4475.70	0	0
Strain-based	4475.70	0	0
Displacement-based + $\mathcal{N}(0,1)$	4471.10 $\pm$133.13	0.036 $\pm$12.87	0.032 $\pm$15.56
Strain-based + $\mathcal{N}(0,0.04)$	4485.20 $\pm$149.28	0.017 $\pm$8.89	0.026 $\pm$11.59

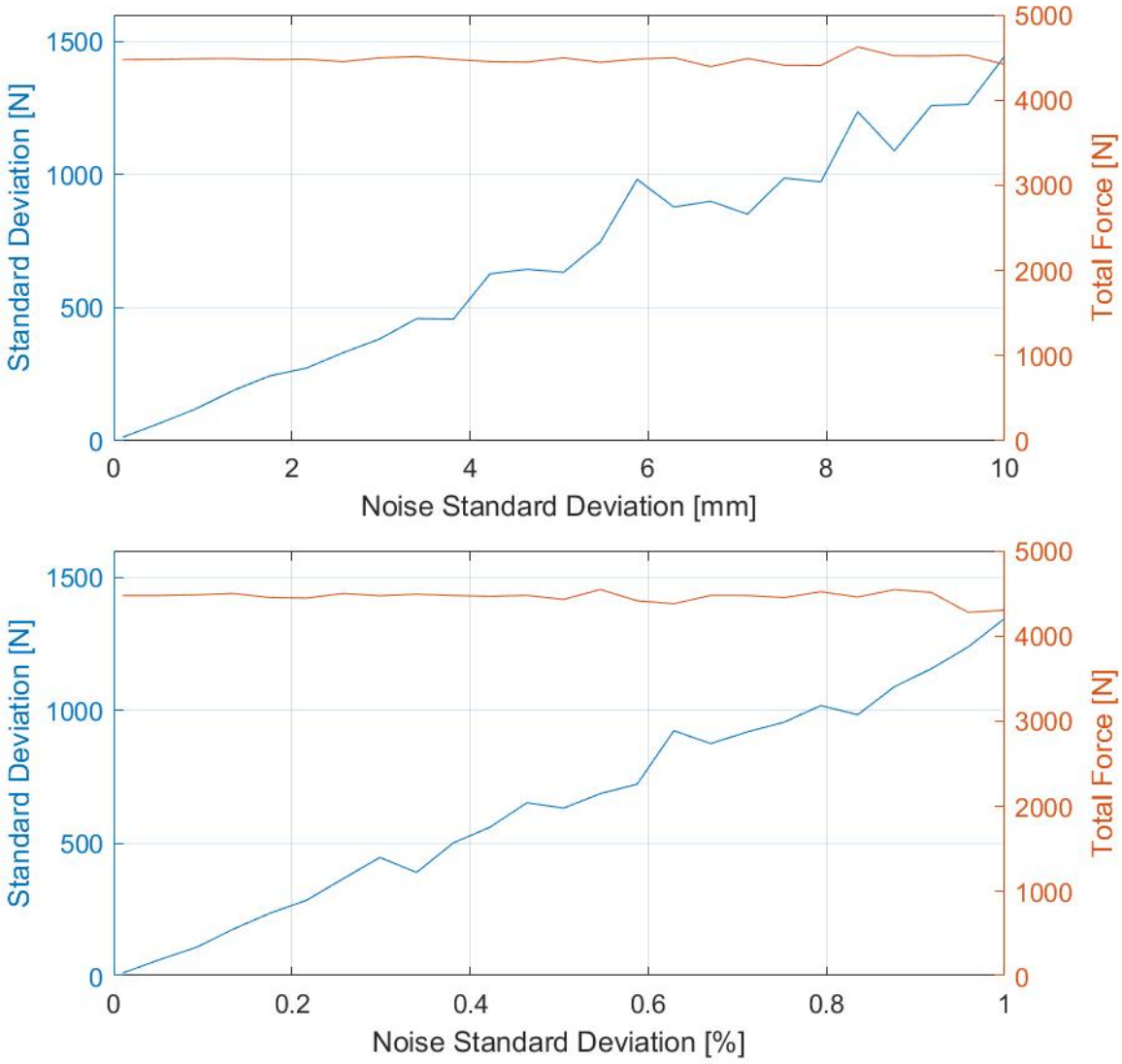

Figure 5.12: Total force and it's standard deviation for various levels of noise with the displacement-based method (top) and strain-based method (bottom)

5.7 Chapter Summary

In this chapter a data-driven approach to analyse the relationship between external forces and internal strains and deformations is presented. A small dataset is generated which is used to find the principal components of the cross-covariance between the external forces and internal strains and deformations. This analysis shows that the first principal component dominates the problem and could be used to reduce the dimensionality. Certain measurement directions are more informative than others, and it is found that vertical deformations and longitudinal strains are the most informative deformation and strain measurements respectively. Certain regions of the tyre are informative about the vertical force in different directions. The displacement measurements have clear regions where each measurement is informative, and these regions have little to no overlap. The strain measurements are all weakly informative in a similar region to one another, and this region is similar to where high strains are observed in laboratory experiments. This analysis shows that there is a clear hierarchy to which measurements are important not only from an experimental perspective, but also in terms of regularization as many regions can be ignored to ease the identifiability of external forces. Moreover, it is clear that deformation is the preferred measurement as it is the most informative of the external forces.

Two methods are presented for using principal components to develop a regression model between the strains or deformations on the inner surface of the tyre and the external forces. The first model is a principal component regression which is a linear model on the principal components of the input and output, while the second is a partial-least squares regression that aligns the directions of the input and output to maximise their correlation. The second method was used to revisit the investigations performed in Section 4 without the effects of the optimisation present. The results were similar: the total forces and moments are readily identified but the distribution of those forces is less identifiable. This data-driven method is much more computationally efficient for investigating the sensitivity of parameters. The sensitivity of the external forces was determined over a range of measurement noise levels instead of on just one noise level as in Section 4. While these data-driven methods presented are not suitable for predicting information outside of their training dataset, they are extremely useful for studying the identifiability of parameters in an inverse problem.

Chapter 6

Conclusions and Recommendations

6.1 Conclusions

An accurate, real-time estimate of tyre force on a vehicle's tyre can be used to develop better Advanced Driver Assistance Systems - however, this is no trivial exercise. A good understanding of the most important dynamics of the tyre and how it produces force is essential to developing such a system. One method to potentially estimate tyre force is with the use of an intelligent tyre, which is a tyre with a sensor system attached to it to measure acceleration, deformation, or strain. Many intelligent tyre concepts have been developed but it is clear that the concepts with the most potential are those which measure displacement or strain on the inner surface of the tyre. One such system was developed at the University of Pretoria, called the Tyre-Terrain Camera (T2Cam), and makes use of a stereo camera arrangement to measure the full-field strain and displacement fields of the inner carcass of a rolling tyre. This camera system is unique since all other intelligent tyre concepts measure acceleration, strain, or displacement at only one point or along a line. The capability therefore exists to extract large amounts of meaningful data from the tyre during operation, but a method has not been developed to relate the measured strain and displacement fields to the force distribution applied externally to the tyre.

There is a lot of uncertainty in the problem of modelling tyre force without knowing the boundary conditions at the tyre-road interface, and this problem constitutes one that is not only an inverse problem but also an ill-posed one. Guides exist in literature for best-practise approaches

to similar problems to help guide the solution. In one such situation, it is often best to choose either the simplest possible model, or the model which most accurately captures the physics of the problem. As a research tool one must always choose the option with the most potential and therefore two physical models were developed to investigate whether or not tyre forces can be identified from measurements taken inside the tyre. A open-source FEM code (CalculiX) was chosen to develop these models - one with simplified boundary conditions to expose the sensitivity of the problem and another which was shown to capture the most important behaviour of a real tyre. The simplified model could not be validated against some experimental data, but the model representative of a real tyre was shown to have the same macroscopic force-displacement characteristics as the tyre it was modelled after. Both models were used to generate virtual experiments for the analysis of the inverse problem that followed, and this allowed for one to better understand the performance of the inverse methods as the true answers are always known.

The model with simplified boundary conditions was used to explore the possibility of identifying external forces using a naïve unconstrained optimisation algorithm. Internal strain and deformation were used separately in two different objective functions for the optimisation, which allowed for comparisons between the two measurement options available with T2Cam. Under ideal conditions the individual external forces can readily be identified and therefore the total force predicted was also accurate. When one adds measurement noise representative of reality, then the distribution of identified forces becomes more varied - at individual nodes it is more likely to under- or over-estimate the force. Despite this increase in variance the total forces identified was found to be similar to that of the ideal case. The initial guess used for the optimisation algorithm for both of these studies was 90% of the true answer, and so a study was conducted to better understand how the initial guess affects the distribution of forces identified. If one adds random noise to the initial guess such that the initial guess is still on average correct, then the distribution of identified forces becomes unacceptably poor. This study was repeated using a uniform initial guess where each node was assumed to have the average force in the contact patch, and was found to have similar results. In both cases the total force identified was close to the answer, but the actual shape of the force distribution was not similar. It was found that using strain or displacement as the measurement is largely similar, and the variance in their performance relative to each other was much smaller than the variance due to measurement noise or the initial guess. The severe decline in the identifiability of the shape of external forces is likely due to many local minima that exist in the design space, which

makes it difficult for the optimisation to tell the difference between many solutions that have the same total force. This is a clear demonstration of Saint Venant's principle where any statically equivalent loading produces similar stress or strain fields far away from the load application.

A data-driven approach was shown to be highly effective at identifying trends in the tyre's behaviour. A simple principal component analysis was applied on the external forces and internal nodal strains and deformations on a small dataset. This principal component analysis revealed that certain regions of the inside of the tyre are more informative than others, and also that these regions differ between strain and deformation as well as the directions of each. Strain was found to be on average weakly informative compared to deformation. The unconstrained optimisation approach failed to identify external forces, but the principal component analysis shows that there is a single latent variable that explains the majority of the variance in the external forces. Thus, this type of analysis is well suited to further develop intelligent tyre models, appropriate regularization strategies and to inform further development of the measurement technology. Furthermore Principle Component Regression and Partial-Least Squares Regression were used to show that although a single latent variable can be identified in the dataset, it requires at least 3 principle components to model the non-linearity inherent in the tyre. The identifiability study was repeated with Partial Least-Squares Regression in a way that removes the effect of the initial guess. The results were similar to that of the identifiability study in that the total external force is readily identifiable, while the distribution is less so. This method requires far less computational time and as such allows for producing a large dataset relatively quickly, which was used to map the identifiability of external forces at each location of the contact patch. Finally, this approach was extended to show the relationship between the identifiablity of the external forces against the noise level of internal strain or deformation.

6.2 Recommendations

A naïve approach to estimating tyre forces is unlikely to yield a trust-worthy estimate of the distribution of forces. It is clear that some regularization strategy must be implemented, and it is shown that not all of the measurements need be considered. It is recommended to re-formulate the objective functions used in the optimisation to only consider the regions which are most informative, which would prevent situations where weakly informative nodes make it more difficult to distinguish between different solutions.

The models developed in Section 3 were developed with expert guidance and previous research to capture the model essential physics related to tyre behaviour for this study, but it is unknown if this model accurately represents local tyre behaviour. Similarly, it is not known if the model captures significant complexity in order to be extended to lateral and longitudinal studies with friction or studies where the tyre is in motion. The full geometry model that was developed correlated well with macroscopic experimental results, but one cannot use this to guarantee that the strains and deformations found to be informative in Section 4 are represented well locally. It is recommended that a more extensive sensitivity study is conducted to rank how model complexity increases in terms of representing local tyre behaviours as well as it's performance when friction and more complicated loadings are applied.

This study was completed without performing the virtual inverse simulation on real test data from T2Cam. Virtual experiments allow for tightly controlling the parameters of interest, but it is important to ensure that the theoretical analysis can predict forces from an appropriate laboratory test before more complexity is added. The friction in the contact patch in a quasi-static vertical stiffness versus vertical deformation test has minimal effect on the total forces, but the "squirming" effect caused by friction may be important to model in order for the inverse analysis to work in reality.

The PCA performed was shown to be a useful tool to better understand how much information the measurements actually contain. This study did not include friction or lateral and longitudinal loadings, so it is recommended that virtual experiments be generated for these loadings and the PCA repeated. PCA was shown to readily identify a single latent variable in a one-dimensional virtual experiment dataset, so this study should be extended to include

more loading scenarios to determine if the same tools can identify these load cases. This study would be helpful to formulate regularization strategies for the types of measurements that an intelligent tyre would capture. Similarly, one can repeat the PLSR investigation with more complicated loadings to determine parameter sensitivity more broadly.

The intelligent tyre that this study was tailored for measures full-field strain and deformation on the inner surface of the tyre. Since the whole inside of the tyre's geometry is known, one can offset this geometry by the tyre thickness and apply this outer geometry as a boundary condition to a FEM model. Such a method would constitute a regularization strategy which is based on the reality of the measurements, rather than some assumptions made upfront. It is recommended that such a regularization strategy be implemented and compared to the work done in this study.

Ultimately it is desirable to predict the distribution of external forces acting on the tyre, but one requires a physically meaningful initial guess to predict this with a non-linear physical model. This force distribution is far more complicated than typical 1 or 2 parameter statistical distributions, but the methods presented in this study could be used to develop a crude statistical "tyre distribution". Such a distribution could be developed such that it depends on relatively simple parameters and produces a normalized distribution of external forces, which can be used as a model in it's own right or as an initial guess to a non-linear physical model for an intelligent tyre.

Bibliography

Asaadi, E., Wilke, D. N., Heyns, P. S., and Kok, S. (2017). The use of direct inverse maps to solve material identification problems: pitfalls and solutions. *Structural and Multidisciplinary Optimization*, 55(2):613–632.

Becker, C. and Els, S. (2022). Agricultural tyre stiffness change as a function of tyre wear. *Journal of Terramechanics*, 102:1–15.

Ben Turkia, S., Wilke, D. N., Pizette, P., Govender, N., and Abriak, N.-E. (2019). Benefits of virtual calibration for discrete element parameter estimation from bulk experiments. *Granular Matter*, 21(4):1–16.

Brodsky, H. and Hakkert, A. S. (1988). Risk of a road accident in rainy weather. *Accident Analysis & Prevention*, 20(3):161–176.

Chang, Y., El-Gindy, M., and Streit, D. A. (2004). Literature survey of transient dynamic response tyre models. *International journal of vehicle design*, 34(4):354–386.

Conradie, J. M., Els, P. S., and Heyns, P. S. (2016). Finite element modelling of off-road tyres for radial tyre model parameterization. *Proceedings of the Institution of Mechanical Engineers, Part D: Journal of Automobile Engineering*, 230(4):564–578.

De Jong, S. (1993). Simpls: an alternative approach to partial least squares regression. *Chemometrics and intelligent laboratory systems*, 18(3):251–263.

Feldesi, F., Botha, T. R., and Els, P. S. (2020). Full-field strain measurements of the inside of an agricultural tyre using digital image correlation. *Journal of Terramechanics*, 91:309–318.

Gallrein, A. and Bäcker, M. (2007). Cdtire: a tire model for comfort and durability applications. *Vehicle System Dynamics*, 45(S1):69–77.

Garcia-Pozuelo, D., Olatunbosun, O., Strano, S., and Terzo, M. (2019a). A real-time physical model for strain-based intelligent tires. *Sensors and Actuators A: Physical*, 288:1–9.

Garcia-Pozuelo, D., Olatunbosun, O., Yunta, J., Yang, X., and Diaz, V. (2017a). A novel strain-based method to estimate tire conditions using fuzzy logic for intelligent tires. *Sensors*, 17(2):350.

Garcia-Pozuelo, D., Olatunbosun, O. A., Romano, L., Strano, S., Terzo, M., Tuononen, A. J., and Xiong, Y. (2019b). Development and experimental validation of a real-time analytical model for different intelligent tyre concepts. *Vehicle system dynamics*, 57(12):1970–1988.

Garcia-Pozuelo, D., Yunta, J., Olatunbosun, O., Yang, X., and Diaz, V. (2017b). A strain-based method to estimate slip angle and tire working conditions for intelligent tires using fuzzy logic. *Sensors*, 17(4):874.

Gere, J. and Goodno, B. (2009). Mechanics of materials.

Geuzaine, C. and Remacle, J.-F. (2009). Gmsh: A 3-d finite element mesh generator with built-in pre-and post-processing facilities. *International journal for numerical methods in engineering*, 79(11):1309–1331.

Gipser, M. (2007). Ftire–the tire simulation model for all applications related to vehicle dynamics. *Vehicle System Dynamics*, 45(S1):139–151.

Gipser, M. (2016). Ftire and puzzling tyre physics: teacher, not student. *Vehicle System Dynamics*, 54(4):448–462.

Guido Dhondt, Klaus Wittig (1998). *CalculiX: A Three-Dimensional Structural Finite Elemente Program*.

Guthrie, A. G. (2016). *3D Computer Vision Contact Patch Measurements Inside Off-Road Vehicle Tyres*. Master's thesis, University of Pretoria.

Guthrie, A. G., Botha, T. R., and Els, P. S. (2017). 3d contact patch measurement inside rolling tyres. *Journal of Terramechanics*, 69:13–21.

Hirschberg, W., Rill, G., and Weinfurter, H. (2007). Tire model tmeasy. *Vehicle System Dynamics*, 45(S1):101–119.

Holtschulze, J., Goertz, H., and Hüsemann, T. (2005). A simplified tyre model for intelligent tyres. *Vehicle System Dynamics*, 43(sup1):305–316.

Khaleghian, S., Emami, A., and Taheri, S. (2017). A technical survey on tire-road friction estimation. *Friction*, 5(2):123–146.

Khaleghian, S., Ghasemalizadeh, O., and Taheri, S. (2016). Estimation of the tire contact patch length and normal load using intelligent tires and its application in small ground robot to estimate the tire-road friction. *Tire Science and Technology*, 44(4):248–261.

Khaleghian, S., Ghasemalizadeh, O., Taheri, S., and Flintsch, G. (2019). A combination of intelligent tire and vehicle dynamic based algorithm to estimate the tire-road friction. *SAE International Journal of Passenger Cars-Mechanical Systems*, 12(2):81–98.

Lee, H. and Taheri, S. (2019). A novel approach to tire parameter identification. *Proceedings of the Institution of Mechanical Engineers, Part D: Journal of Automobile Engineering*, 233(1):55–72.

Li, B., Yang, X., and Yang, J. (2014). Tire model application and parameter identification-a literature review. *SAE International Journal of Passenger Cars-Mechanical Systems*, 7(2014-01-0872):231–243.

Matsuzaki, R., Hiraoka, N., Todoroki, A., and Mizutani, Y. (2010). Analysis of applied load estimation using strain for intelligent tires. *Journal of Solid Mechanics and Materials Engineering*, 4(10):1496–1510.

Mendoza-Petit, M., García-Pozuelo, D., Díaz, V., and Olatunbosun, O. (2020). A strain-based intelligent tire to detect contact patch features for complex maneuvers. *Sensors*, 20(6):1750.

Oertel, C. and Fandre, A. (2009). Tire model rmod-k 7 and misuse load cases. Technical report, SAE Technical Paper.

Oertel, C. and Hempel, J. (2014). Smart tire: a pattern based approach using fem. In *10th Annual Conference Intelligent Tire Technology*.

Pacejka, H. (2005). *Tire and vehicle dynamics*. Elsevier.

Pacejka, H. B. and Bakker, E. (1992). The magic formula tyre model. *Vehicle system dynamics*, 21(S1):1–18.

Pegram, M. S., Botha, T. R., and Els, P. S. (2021). Full-field and point strain measurement via the inner surface of a rolling large lug tyre. *Journal of Terramechanics*, 96:11–22.

Stallmann, M. J. and Els, P. S. (2014). Parameterization and modelling of large off-road tyres for ride analyses: Part 2–parameterization and validation of tyre models. *Journal of Terramechanics*, 55:85–94.

Stallmann, M. J., Els, P. S., and Bekker, C. M. (2014). Parameterization and modelling of large off-road tyres for ride analyses: Part 1–obtaining parameterization data. *Journal of terramechanics*, 55:73–84.

Svensén, M. and Bishop, C. M. (2007). Pattern recognition and machine learning.

The European Commission (2005). Intelligent tyre for accident-free traffic. Finland. `https://cordis.europa.eu/project/id/IST-2001-34372`.

The European Commission (2008). On-board measurement of friction and road slipperiness to enhance the performance of integrated and cooperative safety systems. Finland. `https://cordis.europa.eu/project/id/027006`.

The Mathworks, Inc. (2020). *MATLAB version 9.8.0.1323502 (R2020a)*. Natick, Massachusetts.

Tsiotras, P. and De Wit, C. C. (2000). On the optimal braking of wheeled vehicles. In *Proceedings of the 2000 American Control Conference. ACC (IEEE Cat. No. 00CH36334)*, volume 1, pages 569–573. IEEE.

Tuononen, A. (2009). On-board estimation of dynamic tyre forces from optically measured tyre carcass deflections. *International journal of heavy vehicle systems*, 16(3):362–378.

Van Oosten, J., Unrau, H.-J., Riedel, A., and Bakker, E. (1997). Tydex workshop: standardisation of data exchange in tyre testing and tyre modelling. *Vehicle System Dynamics*, 27(S1):272–288.

Wilke, D. N., Kok, S., and Groenwold, A. A. (2010). The application of gradient-only optimization methods for problems discretized using non-constant methods. *Structural and Multidisciplinary Optimization*, 40(1):433–451.

Xu, N., Askari, H., Huang, Y., Zhou, J., and Khajepour, A. (2020). Tire force estimation in intelligent tires using machine learning. *arXiv preprint arXiv:2010.06299*.

Yang, X., Olatunbosun, O., Garcia-Pozuelo, D., and Bolarinwa, E. (2015). Fe-based tire loading estimation for developing strain-based intelligent tire system. Technical report, SAE Technical Paper.

Yunta, J., Garcia-Pozuelo, D., Diaz, V., and Olatunbosun, O. (2018). A strain-based method to detect tires' loss of grip and estimate lateral friction coefficient from experimental data by fuzzy logic for intelligent tire development. *Sensors*, 18(2):490.